J. Phys. C: Solid State Phys. **18** (1985) 5549–5578. Printed in Great Britain

Measurements of ultrasonic attenuation and velocity in Verneuil-grown and flux-grown $SrTiO_3$

J O Fossum† and K Fossheim

Department of Physics and Mathematics, The Norwegian Institute of Technology, 7034 Trondheim-NTH, Norway

Received 13 July 1984, in final form 18 February 1985

Abstract. Ultrasonic attenuation and velocity have been studied above the 105 K structural phase transition in $SrTiO_3$. Two different samples, one Verneuil-grown, the other flux-grown, have been investigated. The data were analysed self-consistently to obey symmetry requirements and the Kramers–Kronig relations. Both samples possess the same power law behaviour for the measured quantities. The exponents are larger than the critical exponents predicted from renormalisation group theory. An order of magnitude difference in relaxation time amplitudes between the two samples is interpreted as being due to different impurity contents. In the flux-grown sample, first-order-like behaviour was observed.

1. Introduction

The perovskites ABX_3 represent important model systems in the context of modern critical phenomena. Many cubic perovskites undergo structural phase transitions which are connected to the near freezing out of a soft phonon with rotations of X-ion octahedra as the basic motion (Müller 1971).

Measurements of the stress–temperature phase diagrams in perovskites have emphasised the importance of treating order parameter fluctuations properly in theoretical descriptions. Classical Landau theory does not describe the static asymptotic critical behaviour in cubic perovskites. For instance unstressed $KMnF_3$ (Stokka and Fossheim 1981), and possibly also unstressed $SrTiO_3$ (Müller 1982), possess so called fluctuation driven first-order transitions (Aharony and Blankschtein 1984, Blankschtein and Aharony 1981).

Early experimental investigations have been reviewed by, for instance, Müller (1971), while Bruce and Cowley (1981) have given an extensive presentation of experiments and theory for perovskites and other structural systems. Recent results on multicritical phenomena in perovskites were reviewed by Aharony and Blankschtein (1984), Blankschtein and Aharony (1981), Müller *et al* (1984) and Fossheim (1984).

Experiments have revealed two distinct timescales close to and above the transitions in cubic perovskites. One relaxation time is connected to the dynamics of the overdamped soft phonon, while the other one is slower and appears in scattering experiments as a

† Present address: Department of Chemistry and Center for Materials Science and Engineering, Massachusetts Institute of Technology, Cambridge, Massachusetts 02139, USA.

0022-3719/85/295549 + 30 $02.25

narrow peak centred at zero-frequency shift. The latter timescale may be due to defects, but intrinsic mechanisms have also been suggested (Müller 1981).

In the present paper extensive ultrasound attenuation and velocity data are presented and discussed on the basis of measurements at various frequencies and modes in two different kinds of $SrTiO_3$ crystals, in an attempt to obtain a better understanding of the critical behaviour in perovskites.

A phenomenological theory of sound velocity and attenuation above T_c in cubic perovskites was presented in § 8 of the preceding theoretical paper (Fossum 1985), and will not be repeated here. The most important conclusions to be drawn from the theoretical results are, when contributions from the non-symmetry-breaking 'expansion' modulus are neglected:

(i) The critical part of the sound velocity, Δv, should behave according to a single power law $\omega^0 t^{-\mu}$ (possibly a sum of two power laws) well above T_c where $\omega\tau \ll 1$. When $\omega\tau$ becomes greater than unity, a dynamic rollover to $\omega^{-\mu/\nu z} t^0$ behaviour can be expected.

(ii) The critical part of the sound attenuation, $\Delta\alpha$, should behave as $\omega^2 t^{-\rho}$ in the region $\omega\tau \ll 1$ and as $\omega^{2-\rho/\nu z} t^0$ when $\omega\tau \gg 1$. Different sound modes will possess different amplitudes according to symmetry.

The critical parts of the velocity and the attenuation respectively, must be extracted from a total behaviour which also includes background contributions. These are contributions to the complex elastic modulus from non-critical physical processes. Experiments show that well away from critical points both velocity and attenuation behave linearly as a function of temperature (see, for instance, Bjerkan *et al* (1979)). The critical part of the sound attenuation is usually first observed at about $T_c + 10$ K. Thus, the attenuation background which usually depends weakly on temperature may be taken as a constant. The anomalous part of the sound velocity, however, may extend as far as to $T_c + 100$ K. The (usually linear) temperature dependence of the background velocity must be carefully measured and included in the analysis of the data.

The conventional pulse reflection technique for sound attenuation measurements has severe difficulties when measurements are performed close to critical points. The problems which are due to wavefront distortions, may be overcome by means of the phonon echo technique, which has been applied in some of the present measurements.

The phonon echo technique is designed to remove elastic contributions from the sound attenuation. The technique takes advantage of the ability of a backward-propagating phonon echo to reconstruct the wavefront of an applied acoustic wave (see Fossheim and Holt (1982)).

The 105 K phase transition of $SrTiO_3$ has been studied by many techniques. Early ultrasound experiments resulted in partly contradictory results. The present investigation represents the first attempt to measure both velocity and attenuation anomalies at various frequencies and sound modes in the same sample. Some of the early experiments will also be discussed, § 4. Sound velocity has been measured by, for instance, Bell and Rupprecht (1963), Lüthi and Moran (1970), Rehwald (1970, 1977) and Fossheim and Berre (1972). Bell and Rupprecht's results represent the most accurate determination of the background levels. Their results are consistent with the present ones when the uncertainties connected with the pulse overlap technique are taken into account. Lüthi and Moran interpreted the lack of a fluctuation 'dip' at T_c in their measurements, as an indication of negligible fluctuations in $SrTiO_3$. No 'dip' is observed in the present measurements, while Berre and Fossheim (1971) observed a minimum in the sound velocity at T_c when the sample was exposed to compression along the [100] axis. The

most accurate determination of critical sound velocity exponents is found in the papers of Rehwald. We will return to this under the discussion in § 4.

Attenuation measurements close to 105 K in $SrTiO_3$ were published by Berre *et al* (1969), Courdille and Dumas (1969), Rehwald (1970), Nava *et al* (1969), Berre and Fossheim (1971), Fossheim and Berre (1972) and by Domb *et al* (1976). The exponents determined from these experiments vary from $\rho = 0.6$ to $\rho = 3.9$, where the small exponents are found close to T_c (in the rollover region of the present experiments), while the large exponents are revealed away from T_c (see Courdille and Dumas 1969, Rehwald 1970, Berre and Fossheim 1971). Various interpretations have been put forward. For instance, Domb *et al* (1976) interpreted a change in exponents from $\rho = 1.9$ to $\rho = 1.1$ on approaching T_c as a crossover from $d = 2$ to $d = 3$.

Apart from the measurements of Fossheim and co-workers, the frequency dependence of the attenuation has not been studied thoroughly in previous experiments. Thus, dynamical scaling has not been put forward as an explanation to the observed crossover effects. In the measurements of Berre and Fossheim (1971) a frequency-squared dependence was not obtained away from T_c. However, a steep behaviour was observed outside the region which was fitted to single power laws. Important differences between our experimental procedure and earlier ones are firstly that we have been very careful not to cool the samples far below T_c, and secondly the relatively long stabilisation times of the present experiments. For instance, in the early experiments of Fossheim and co-workers, the temperature was not stabilised at all, but was allowed to drift very slowly through the transition. This could possibly account for some of the differences between the earlier results and the present ones.

It is, however, important to note that parts of the reason for the variations in the published results of the exponent ρ is connected with the temperature region in which the data are fitted to an exponent. Some authors have fitted an exponent to the data within what we have termed the rollover region, while others have used data points further away from T_c.

The experimental technique, the samples and mounting of samples is discussed in § 2, while the experimental results are presented in § 3. A summary of the results were published by Fossum and Fossheim (1984), whereas other results on the flux-grown $SrTiO_3$ sample were published by Fossum *et al* (1984).

Since the interpretation of our data is not settled an extensive discussion is given in § 4. Section 5 gives some concluding remarks.

2. Experimental technique and samples

Near phase transitions in solids the sound velocity, v, usually varies strongly with temperature, i.e. $v = v(T - T_c)$ where T_c is the critical temperature. T_c, and therefore also v, is often position dependent due to local defects and strain in the specimen under investigation. This gives rise to acoustic wavefront distortion, i.e. a plane wave transmitted from the transducer may have been strongly distorted before it is detected at a later time. Destructive interference effects may occur, giving rise to oscillatory behaviour of the measured effective sound attenuation as a function of temperature. Non-parallel end faces of the sample can also result in destructive interferences since the sound wavelength $\lambda = 2\pi v/\omega$ is a temperature-dependent quantity. The oscillating attenuation is added to the intrinsic relaxational contributions associated with the phase transition, and thus causes severe problems in the data analysis. The echo method

described below represents a way to get rid of the destructive interferences (see Fossheim and Holt 1982).

In the present experiments, MATEC equipment is used for ultrasonic experiments at frequencies between 10 and 600 MHz. Overtone polished Valpey-Fischer $LiNbO_3$ transducers with fundamental frequencies $\omega_F/2\pi = 15$ or 30 MHz have been employed in our measurements. These transducers are extremely efficient at their resonance frequencies $\omega_R = (2n + 1)\omega_F$ where $n = 0, 1, 2 \ldots$. The efficiency decreases with increasing n, giving a practical upper limit of $n \simeq 10$.

Water-free Nonaq stopcock grease turned out to be most suitable for transducer bonding throughout the temperature region of interest in our measurements. In echo experiments, an echo-active sample must be attached to the sample end opposite to the transducer. In the measurements on $SrTiO_3$ *only* General Electric RTV silicon rubber gave satisfactory acoustic transmission between the two samples at all temperatures of interest. RTV silicon rubber shows a rather abrupt change of mechanical properties at 200 K, giving much better sound transmission below this temperature.

Non-linear electroacoustic interactions in piezoelectrics provide the basis for novel applications in ultrasonic technology. One example is the generation of phonon echoes where an applied forward-propagating acoustic wave $\sim\exp[i(\omega t - \boldsymbol{k}\cdot\boldsymbol{x})]$ interacts with an applied homogeneous electric field ($\sim\exp(-2i\omega t)$ in our experiments) to produce a backward-propagating acoustic wave $\sim\exp[-i(\omega t + \boldsymbol{k}\cdot\boldsymbol{x})]$. The backward-propagating echo represents a replica of the initial, forward-propagating sound wave. The echo generation process gives rise to a reversal of the total wave-vector on each point of the initial wavefront, in contrast to an ordinary reflection from a sample end where only the normal component of the wave-vector is reversed. A plane sound wave transmitted from a transducer will be exposed to both elastic and inelastic (relaxational) scattering. In connection with phase transitions, one is usually only interested in the latter contribution to the sound attenuation, while the elastic scattering gives rise to the problematic wavefront distortions described above.

The phonon echo technique developed by Fossheim and Holt (see, for instance, Fossheim and Holt (1982)) is a method designed to remove the elastic scattering from sound attenuation anomalies. The principle of the method is illustrated in figure 1. The specimen (s) under investigation is attached to an echo-active sample (e). Pulsed sound waves at frequency ω are generated and detected by the resonant transducer bonded to the specimen. The echo sample is placed in a cavity which is tuned at a frequency of 2ω. By mixing of the two signals a phonon echo is generated inside the echo crystal at a position determined by the time interval τ between the application of the field of frequency ω and the RF field of frequency 2ω respectively. The delay time τ is chosen so that the echo is observed between two successive reflections. In this case the other pulses detected at the transducer are due to reflections both from the ends of the specimen (s) and of the echo crystal (e).

The lengths of the two samples must be adjusted so that there is room for observing an echo between the various reflections. This means that $l\,(\mathrm{m}) > 10^{-6}\,\mathrm{s}/v\,(\mathrm{m\,s^{-1}})$ must be fulfilled where v and l are the sound velocity and the length of the specimen respectively, while 10^{-6} s is a typical pulse width in our experiments.

The broadband spiral cavities used in our measurements were developed by Fossheim and Holt (see, for example, Fossheim and Holt 1978).

The frequency, ω, of the applied sound wave is determined by the resonances of the transducer. Second harmonic waves at frequency 2ω (and also higher-order harmonics) are generated both in the transducer and during the wave propagation. These waves can

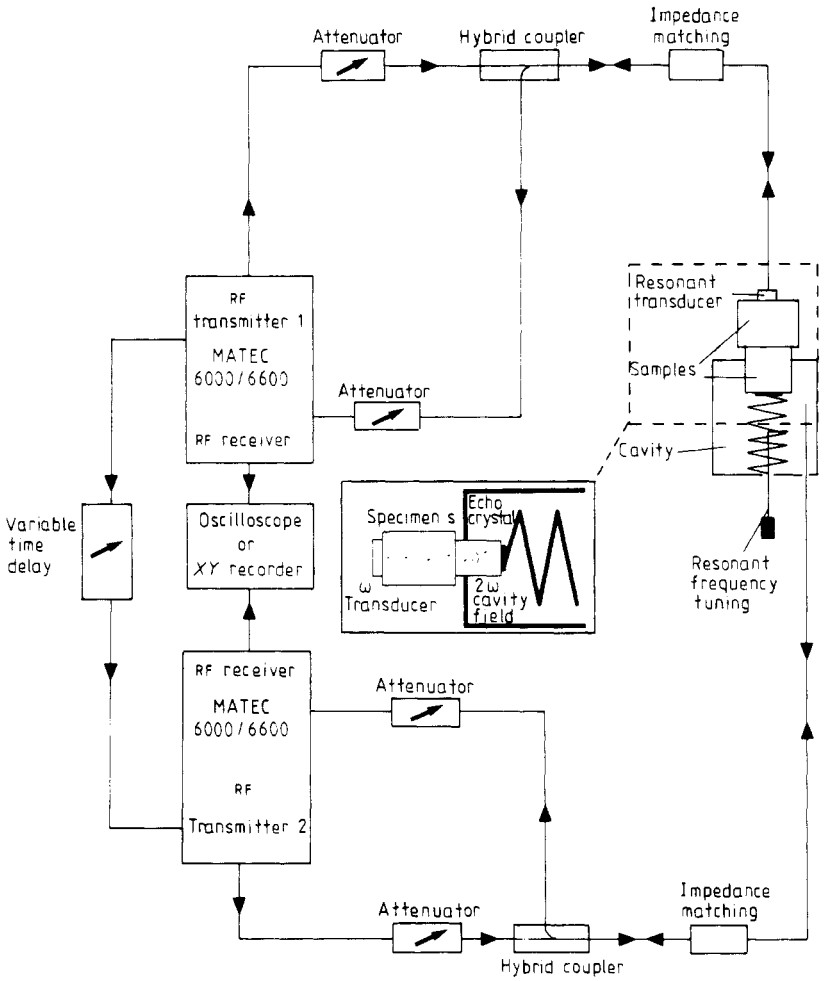

Figure 1. Experimental set-up for attenuation measurements by means of phonon echo technique as well as conventional pulse reflection measurements. The inset is a close-up on the sample/cavity part. The non-echo-active specimen (s) is attached to an echo-active crystal (e). The gradually distorted acoustic wavefront passes into (e), where the wavevector-reversed echo is generated during interaction with the field of frequency 2ω. Adopted from Fossheim and Holt (1982).

be detected in the cavity, and are therefore very useful in tuning the cavity at 2ω. Our most efficient cavities are tunable at all frequencies $2\omega/2\pi > 180$ MHz, which means that echo experiments at sound frequencies $\omega/2\pi > 90$ MHz may be performed with the existing equipment.

In our experiments, the signal-to-noise ratio of the first few reflections of the pulse trains were typically 90–120 dB, while the echo amplitudes were 30–60 dB above the noise level when detected at the transducer. In general, the magnitudes of the signals decreased as a function of increasing frequency. This is mainly due to the transducers which are less efficient when used at higher harmonics. In addition, the background attenuation is proportional to the frequency squared. This sets a practical upper limit for the present echo experiments at $\omega/2\pi \lesssim 300$ MHz. At acoustic frequencies below

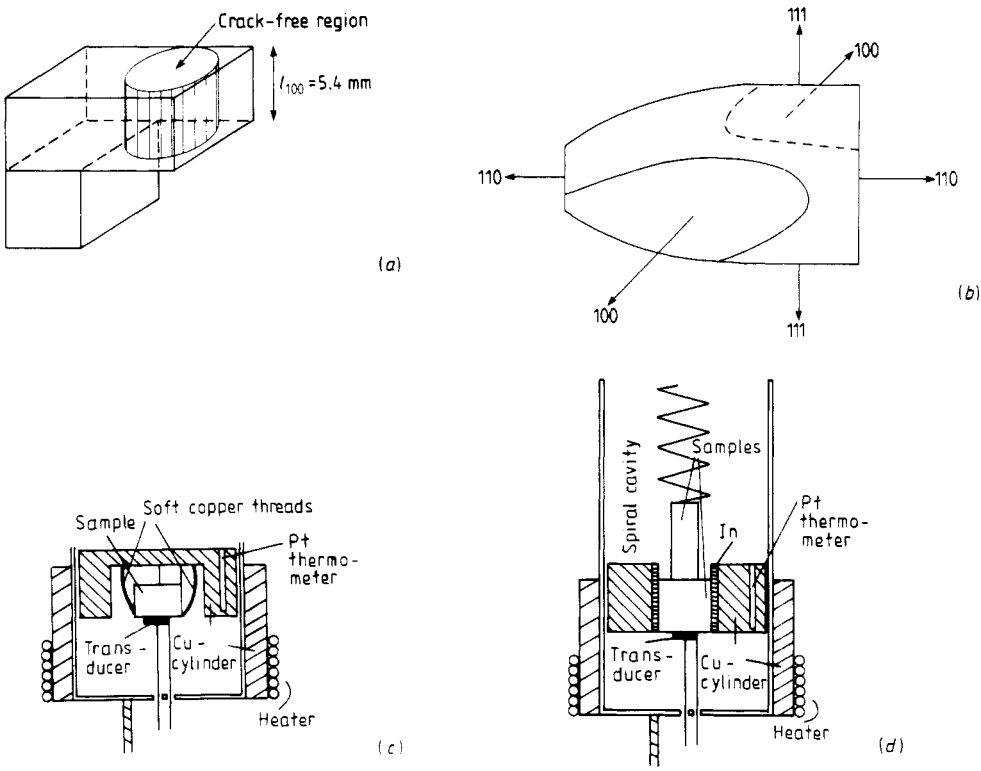

Figure 2. $SrTiO_3$ samples investigated in the experiments. (*a*) Flux-grown sample. The crack-free region investigated is indicated. (*b*) Verneuil-grown sample. Sample dimensions: l_{100} = 2.06 cm; l_{111} = 2.01 cm; l_{110} = 3.05 cm. (*c*) Mounting of flux-grown sample. Nonaq stopcock grease was smeared between the upper edge of the sample and the copper wall. Two soft copper wires were bonded to the top to avoid temperature gradients. (*d*) Mounting of Verneuil-grown sample.

90 MHz and above 300 MHz the conventional pulse reflection technique must be applied.

In the phase transition experiments phonon echo or reflection amplitudes are measured by means of the variable attenuators on the receiver side shown in figure 2. Attenuators on the transmitter and receiver side, respectively were used to control linearity, i.e. to check that the sound attenuation was independent of the applied sound intensity. Amplitude dependence is a sign of breakdown of linear response.

In the present experiment on $SrTiO_3$, the insulating material $Bi_{12}SiO_{20}$ (BSO) was used as an echo material. The echo generation process in BSO was checked to be independent of temperature in the region $100 < T < 120$ K.

Sound velocity was measured by means of the conventional pulse overlap technique (Papadakis 1967). The equipment in our laboratory enabled us to measure the sound velocity in the limited frequency region $10 < \omega/2\pi < 100$ MHz.

In our experiments a system from Linear Research, consisting of an LR-130 temperature controller and an LR-110 resistance bridge was used to control and measure the temperature.

The sample holder was a copper cavity placed in the inner of two concentric dewars.

The sample was usually packed in indium and embedded in a Cu block. Nonaq stopcock grease was applied between the block and the inner wall of the cavity to improve the thermal contact between heater, thermometer and sample. The heater was made from a constantan wire. We used commercial Pt (Rosemount Inc) resistance thermometers with a nearly linear temperature coefficient above 77 K ($R_s = 2000\ \Omega$ at 0 °C).

This system could be controlled such that the temperature was stable to within ±3 mK after 5–10 min of stabilisation.

Two different $SrTiO_3$ crystals were studied in the experiments. One was a flux-grown sample made by Professor Hans J Scheel at the IBM Laboratory in Zürich (sample number 7493), and the other one a Verneuil-grown sample purchased from Commercial Crystal Laboratories Inc.

The shape and dimensions of the flux-grown sample is shown in figure 2(*a*). This sample has naturally grown (100)-surfaces. The colour is dark brownish, and it reveals no macroscopic strains in crack-free regions when placed between crossed polarisers at room temperature. The ultrasound experiments were performed in a crack-free region with approximate volume $7 \times 7 \times 5.4\ mm^3$. Flux-grown crystals of this type are very easily strained when exposed to relatively low stresses. Extreme care is thus required in handling the samples.

In the experiments to be described here, the sample was mounted as shown in figure 2(*c*). The transducer was bonded with Nonaq stopcock grease, which was also smeared under parts of the sample to achieve thermal contact to the surrounding metal walls of the holder. Two soft copper threads were bonded to the top edges to avoid temperature gradients.

Only conventional pulse reflection measurements were performed with the flux-grown sample. There are two main reasons for this. Firstly, the sample was so short that it would be very difficult to detect a phonon echo between the reflections. Secondly, in phonon echo experiments, exercising the required scrupulous care during mounting of the crystal is very difficult. It was decided to avoid the risk of either damaging the crystal while mounting, or introducing anisotropic strains when the temperature was lowered. Hence no treatment, like polishing of surfaces, was done with this sample. This may be the reason for the scatter in the attenuation data.

The shape and the dimensions of the Verneuil-grown sample is shown in figure 2(*b*). This crystal was hard glass-like and transparent and showed *large* amounts of macroscopic strains in crossed polarisers. Three main cubic surfaces were polished ((100), (110) and (111)). The sample was not annealed before the experiments to be described here. The mounting of the Verneuil-grown crystal is shown in figure 2(*d*). Both conventional pulse reflections and phonon echoes were measured. The relatively large dimensions of the sample were necessary to obtain sufficient pulse spacing in the phonon echo measurements.

3. Experimental results

3.1. Sound velocity measurements in flux-grown $SrTiO_3$

Two different sound modes were investigated in the flux-grown sample.

(i) Longitudinal sound parallel to the [100] direction, i.e. $\boldsymbol{q} \parallel \boldsymbol{u} \parallel [100]$, where $\boldsymbol{q}$ and $\boldsymbol{u}$ are the wave-vector and the polarisation of the sound wave respectively. In the velocity measurements, only one frequency was applied: $\omega/2\pi = 20$ MHz.

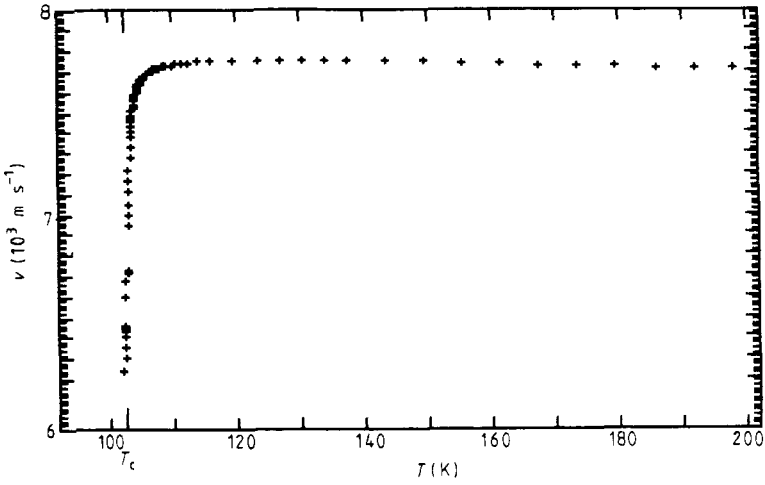

Figure 3. Longitudinal sound velocity v along a cube axis ($\boldsymbol{q} \parallel \boldsymbol{u} \parallel [100]$) in flux-grown $SrTiO_3$ as a function of temperature T. Stabilisation time per measured point was always at least 15–20 min and $\omega/2\pi = 20$ MHz.

(ii) Transverse sound propagating in the [100] direction, i.e. $\boldsymbol{q} \parallel [100]$, $\boldsymbol{u} \perp [100]$. Two frequencies, $\omega/2\pi = 17.5$ MHz and $\omega/2\pi = 85$ MHz, were investigated in this case.

Some of the measurements in the cases (i) and (ii) are shown in figures 3–7. Before plotting all data were corrected for dilatation of the sample according to the data of Golding (1970). The stabilisation time for each point was never less than 15–20 min. Except for measurements shown in figures 5 and 6, T_c was always approached from above. The first measurement on the sample is the one shown in figure 3.

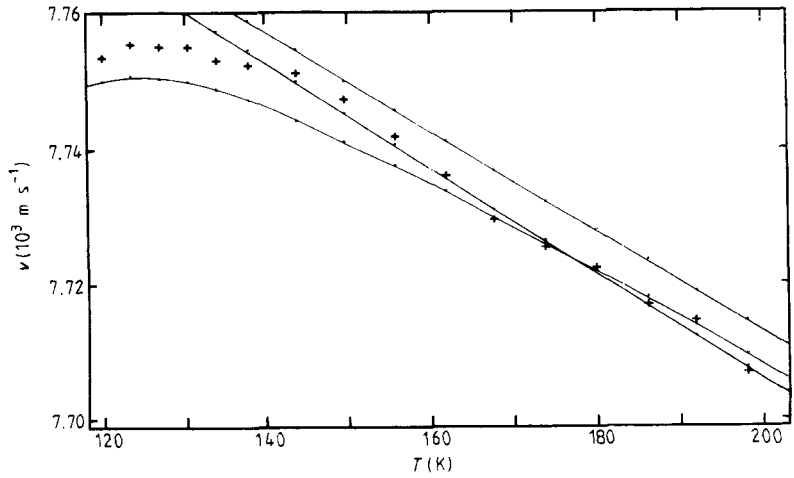

Figure 4. Inspection of the linear background of the measurement shown in figure 3. The fully straight lines represent two different choices of linear background. The upper one is determined from fitting *all* data above $T_c + 0.3$ K to a straight line plus an anomalous single power law, resulting in the *smooth curve* mostly under the measured points. The lower straight line is a linear regression fit to all measured points above 140 K.

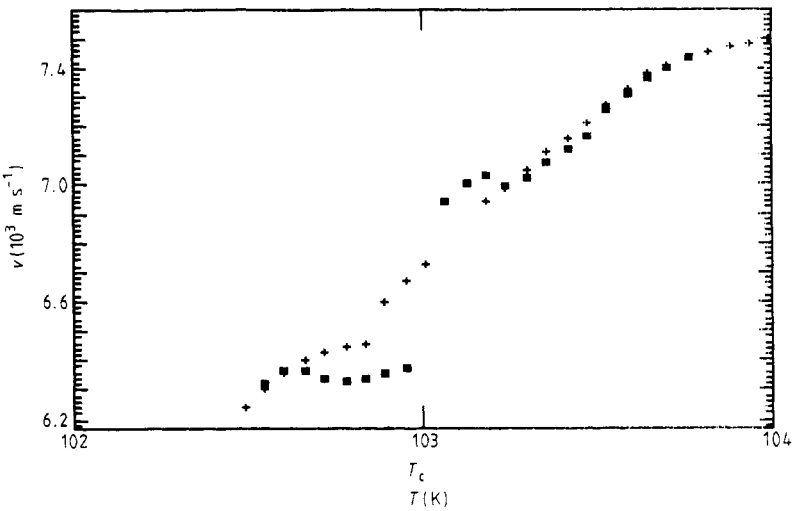

Figure 5. Close-up of the behaviour near T_c of the measurements shown in figure 3. Note the steps and the hysteresis. The data are +, decreasing temperature; ■, increasing temperature.

The expanded plot in figure 5 shows a step at T_c, and hysteresis, a sign of first-order character of the transition. The behaviour close to T_c, above and below, was measured twice in addition to the run plotted here. The data in figure 5 were reproduced in each case, except below T_c, where it took a much longer time to reach equilibrium than above the transition. As a function of decreasing temperature, this qualitative difference between the two phases was revealed exactly at the step shown in figure 5. Some points are missing in figure 5. This is due to destructive interference effects which completely destroyed the second reflection of the pulse train in this temperature region.

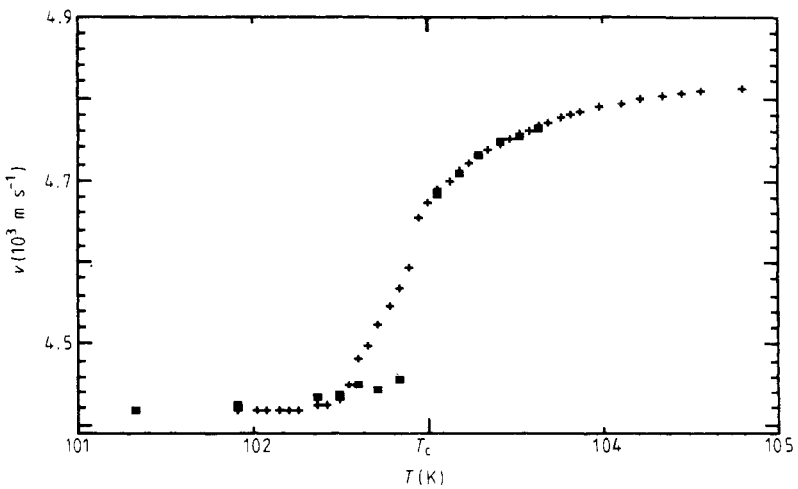

Figure 6. Close-up of behaviour near T_c of the transverse sound velocity, v, as a function of temperature, T, along a cube axis in flux-grown $SrTiO_3$. Stabilisation time per point always at least 20 min. Note the steps and the hysteresis. $\boldsymbol{q} \parallel [100]$, $\boldsymbol{u} \perp [100]$, $\omega/2\pi =$ 17.5 MHz. The data are +, decreasing temperature; ■, increasing temperature.

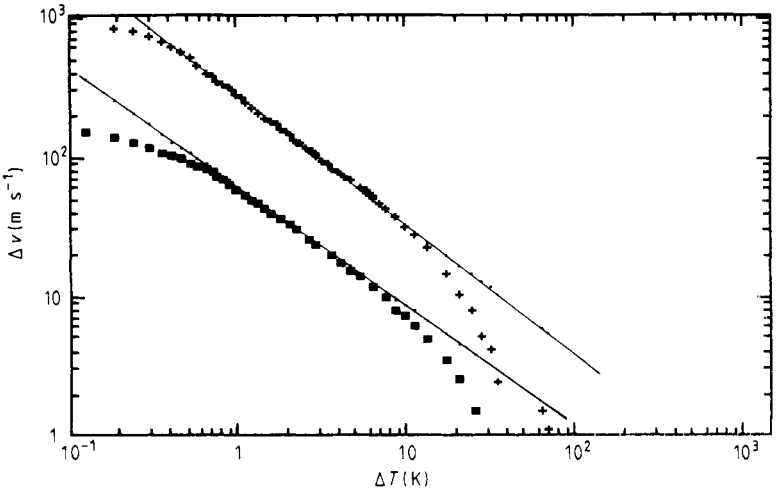

Figure 7. Log–log plots of the anomalous (critical) parts of longitudinal and transverse sound velocities along a cube axis in flux-grown $SrTiO_3$. $T_c = 103.5$ K, while the background is chosen as the linear regression on points above 140 K for both modes. The straight lines drawn here are obtained from fitting all the points between 0.3 K (0.7 K for the transverse mode) and 10 K to the linear background plus a single power law. The results are $\mu = 0.86$ in the transverse case while $\mu = 0.93$ for the longitudinal mode. The data are: +, $\boldsymbol{q} \| \boldsymbol{u} \| [100]$, $\omega/2\pi = 20$ MHz; ■, $\boldsymbol{q} \| [100]$, $\boldsymbol{u} \perp [100]$, $\omega/2\pi = 17.5$ MHz.

Well above the transition a linear background behaviour was obtained as shown in figure 4. By choosing the background as the straight line resulting from a linear regression fit to all points above 140 K, and choosing T_c approximately at the mid-point of the hysteresis, i.e. $T_c = 103.0$ K, one obtains figure 7. The slope of the straight line between $\Delta T \sim 0.3$ K and $\Delta T \sim 15$ K in figure 7 is determined as $\mu \sim 0.8$–0.9 by simple inspection. Since a nice straight line is obtained over one and a half decades in the log–log plot, the velocity measurements were fitted to a single power law. No correction to scaling terms or other corrections have been considered.

The measured points in the temperature region $0.3 < \Delta T < 15$ K may then be described by the function

$$v = A_1 - A_2 T - C(T - T_c)^{-\mu} \tag{1}$$

where $A_1 - A_2 T$ is the background, C is the amplitude of the anomalous part, Δv, and μ is the critical exponent. The data points of the longitudinal wave between 0.3 K and 15 K in figure 7 were fitted to equation (1) in four different manners.

(*a*) Only C and μ were allowed to vary, while A_1, A_2 and T_c were fixed at the values determined from simple inspection.

(*b*) C, μ, A and A_2 were treated as free parameters, while only T_c was kept constant.

(*c*) C, μ and T_c were free, and the background variables A_1 and A_2 were fixed at their linear regression values.

(*d*) *All* five parameters A_1, A_2, C, μ and T_c were allowed to vary. The freely moving background parameters A_1 and A_2 and the transition temperature T_c were found to coincide with their respective fixed values within experimental error.

As a fifth approach (*e*) *all* the measured points above 0.3 K were fitted to equation (1) with all five parameters free.

Some of the measured points of the two different frequencies for the transverse sound mode along the [100] direction are plotted in figure 6 and in Fossum *et al* (1984). The steps and the hysteresis close to T_c appeared just as in the longitudinal case. No frequency dependence of the sound velocity was revealed from these experiments. The qualitative difference in stabilisation time discussed above for the longitudinal wave, was also present in this case, i.e. above T_c the measured signals were stable when the temperature was stabilised, while below the transition, the signal showed a drift, although the temperature was stable. The sample has never been taken further down below T_c than shown in the measurement of figure 6.

By choosing the background as the linear regression line given by measurements above 140 K, and by choosing $T_c = 103.0$ K at the mid-point of the hysteresis, one obtains the lower log–log plot shown in figure 7. A fit of equation (1) to the points in the region $0.7 < \Delta T < 10$ K yielded an exponent $\mu = 0.86$ and an amplitude $\Delta v(\Delta T = 1\text{ K}) = 61.5\ \text{m s}^{-1}$. A fit of equation (2) to all the points above $T_c + 0.7$ K gave the results $\mu = 0.83$, $\Delta v(\Delta T = 1\text{ K}) = 60.4\ \text{m s}^{-1}$ and $T_c = 102.98$ K.

All the results discussed above will be summarised below. Here we will only note that $\mu = 0.89 \pm 0.06$ when including the results from all the fitting approaches for both modes.

There are two main conclusions to draw with respect to the uncertainties in this case: firstly, the results within one decade $1 < \Delta T < 10$ K are relatively unaffected by uncertainties in the background *and* in T_c, i.e. the straight-line behaviour within this decade is preserved. Secondly, one may conclude that the rollover close to T_c and the steeper slope of the log–log plots at the highest temperatures are significant effects, which do *not* depend on uncertainties in T_c or the background.

Note that the rollover close to T_c occurs at a higher temperature for the transverse mode than for the longitudinal one (see figure 12). This could be caused by the positioning of the transducer, which was placed very close to one edge of the sample in the transverse case. Since no frequency dependence is observed (see Fossum *et al* 1984), the rollover close to T_c must be considered as a static effect, which is then not due to the dynamic saturation of the sound velocity predicted from the theory of Fossheim and Fossum (1984) and Fossum (1984). Below we will argue that it is important to consider this pure static deviation from the single power law behaviour in the interpretation of the attenuation data.

3.2. Sound velocity measurements in Verneuil-grown $SrTiO_3$

In the Verneuil-grown sample, four different sound modes were investigated. The results are shown in figures 8 to 12.

T_c was difficult to locate in this case. Neither of these velocity experiments nor the attenuation measurements to be discussed below could determine T_c accurately. Stokka and Fossheim (1982) measured the heat capacity on a small sample which was cut from one edge of the present one. The heat capacity measurements gave $T_c = 104.9 \pm 0.1$ K at zero external pressure. Therefore we chose $T_c = 104.9$ K in all the plots shown here.

For all the longitudinal modes, the second reflection, and in some cases also the first reflection, in the pulse-train disappeared at some temperature above 104.9 K during cooling runs. The only case where it was possible to follow the signal through the transition was for the transverse mode. However, the smooth curve plotted in figure 10 reveals no sign of T_c. No time-dependent effects were observed in this case.

Background velocities are chosen as shown in figure 9. The resulting log–log plots of

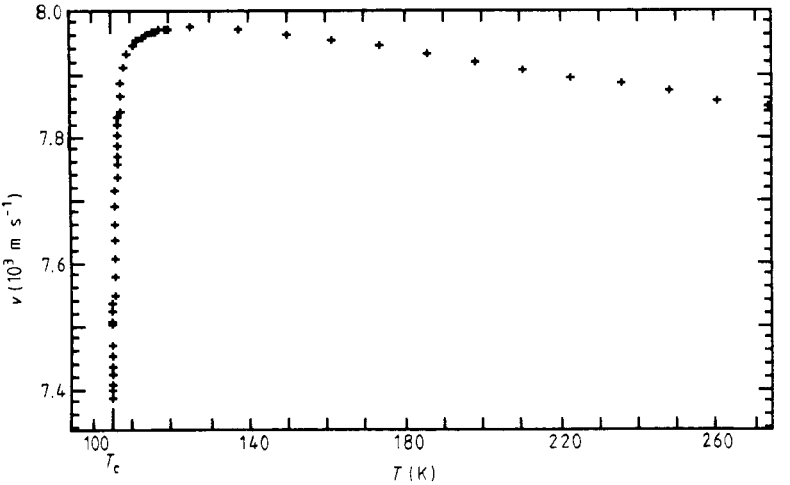

Figure 8. Longitudinal sound velocity, v, along the [100] ($\boldsymbol{q} \| \boldsymbol{u} \| [100]$) direction as a function of decreasing temperature, T, in Verneuil-grown $SrTiO_3$. $\omega/2\pi = 33$ MHz. Stabilisation time per point: 15 min minimum. Also soo figure 9.

the anomalous velocity, Δv, as a function of the relative temperature, ΔT, are shown in figure 11. The curves are not as smooth and straight as those obtained for the flux-grown sample. This is probably due to the macroscopic strains in the present sample. Curve-fitting procedures similar to those discussed in the previous section did not seem worthwhile here. The important thing to learn from the velocity measurements on the Verneuil-grown sample, is that the qualitative features observed in the experiments on the flux-grown sample are preserved. By simple inspection one obtains $\mu \simeq 0.9$ from figure 11 for all the modes plotted, while the transverse mode shown in figure 12 could possess a larger exponent.

In figure 12 a comparison between the two samples is shown.

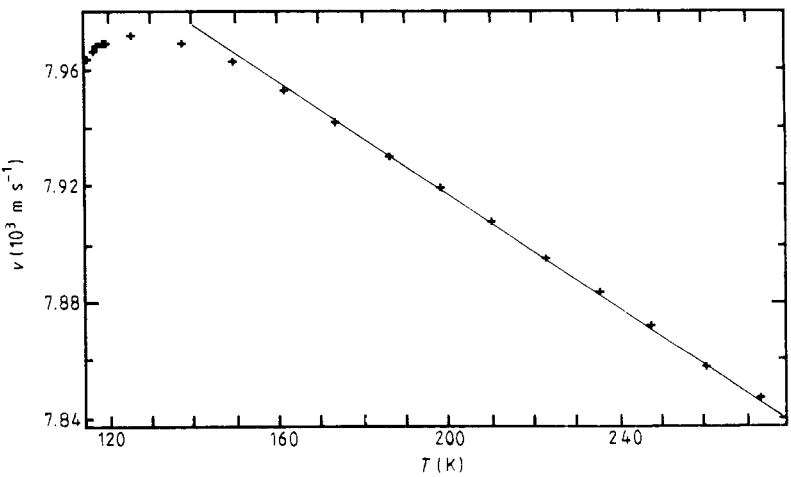

Figure 9. Enlargement of the linear background of the measurements shown in figure 8. The straight line is determined from a linear regression fit to all points above 140 K. The sample is Verneuil-grown $SrTiO_3$, $\boldsymbol{q} \| \boldsymbol{u} \| [100]$, $\omega/2\pi = 33$ MHz.

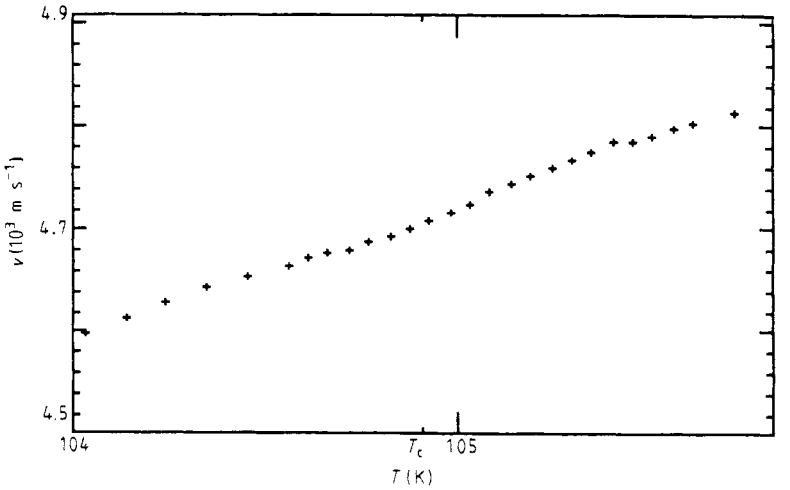

Figure 10. Inspection of the behaviour close to the transition of transverse sound along the [100] direction in Verneuil-grown $SrTiO_3$. The present measurement is the one where the sample was cooled furthest down below T_c ($T_c - 5$ K). $q \parallel [100]$; $u \perp [100]$; $\omega/2\pi = 16$ MHz.

3.3. Sound attenuation measurements in flux-grown $SrTiO_3$

As in the velocity measurements, two sound modes were investigated in the flux-grown sample, namely the longitudinal and transverse waves along one [100] direction. Only a conventional pulse reflection technique was used, for reasons explained in § 2. The data plotted in figure 13 are those for the longitudinal case at $\omega/2\pi = 20$ MHz. Three different runs revealed a maximum of the critical attenuation at $T_c = 103.0 \pm 0.1$ K. The shape of the curve, showing a much steeper behaviour below T_c than above, was reproduced in all the runs, and was independent of whether T_c was approached from above or from

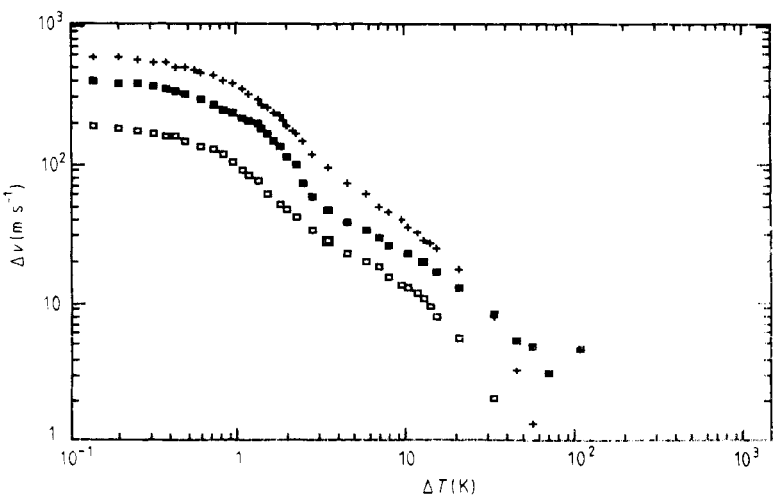

Figure 11. The critical parts of the longitudinal sound velocities along the [100], [110] and [111] directions in Verneuil-grown $SrTiO_3$. $T_c = 104.9$ K, while the respective backgrounds are chosen as indicated in figure 9. The data are: +, $q \parallel u \parallel [100]$, $\omega/2\pi = 33$ MHz; ■, $q \parallel u \parallel [110]$, $\omega/2\pi = 30$ MHz; □, $q \parallel u \parallel [111]$, $\omega/2\pi = 32$ MHz.

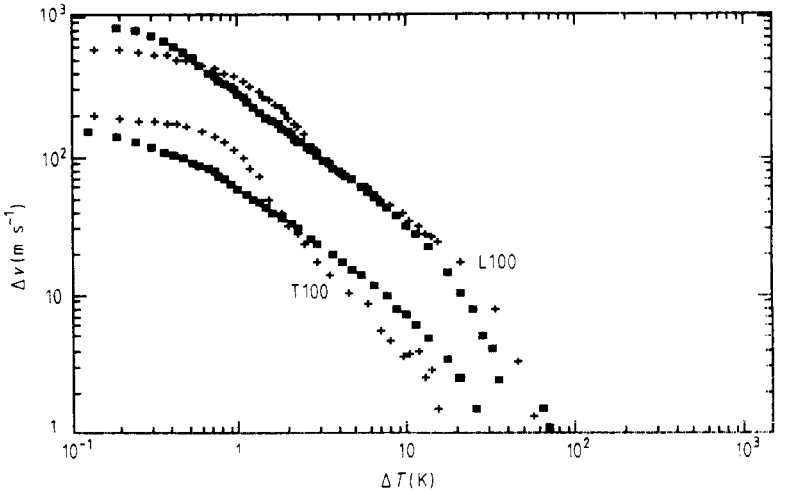

Figure 12. Comparison of critical sound velocities measured in flux-grown (■) and Verneuil-grown (+) $SrTiO_3$.

below. The second increase in the attenuation starting at about $T_c - 0.3$ K, is interpreted as the Landau–Khalatnikov contribution (Landau and Khalatnikov 1951). This will not be discussed further, since no other measurements were performed below T_c. The background levels are believed to be determined within ± 1 dB cm^{-1}. The background is in each case, within experimental error limits, chosen as the zero levels in figure 14. Log–log plots of the critical attenuation, $\Delta\alpha$, against temperature $\Delta T = T - 103.0$ K, are given in figures 15 and 16. The qualitative features are striking: a very steep increase in the attenuation is revealed away from T_c, whereas saturation at a plateau is obtained on approaching the transition. A simple ruler and pencil inspection of the log–log plots

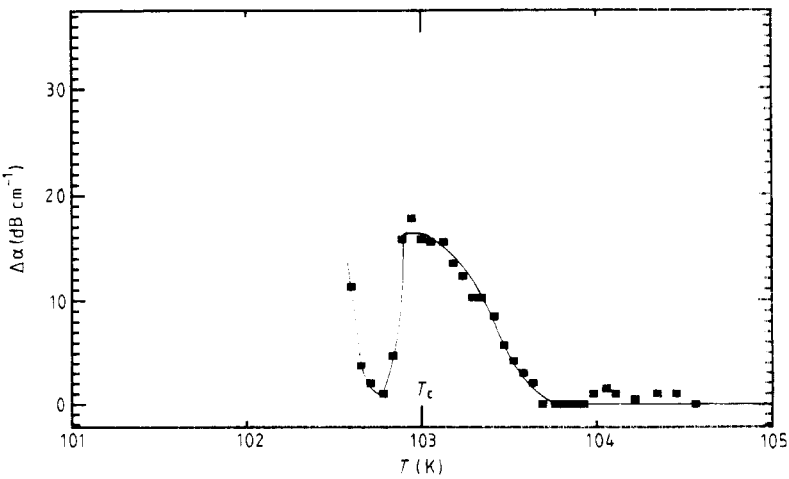

Figure 13. Critical sound attenuation for longitudinal sound propagating in the [100] direction at $\omega/2\pi = 20$ MHz in flux-grown $SrTiO_3$. The full curve is determined from the plotted data and two other runs. The behaviour is independent of whether T_c is approached from above or from below.

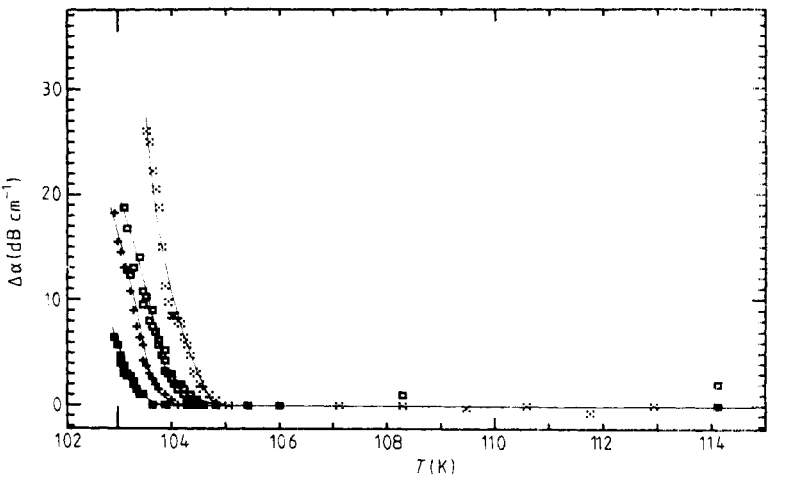

Figure 14. Sound attenuation, $\Delta\alpha$, plotted against temperature, T, for transverse waves along the [100] direction in flux-grown $SrTiO_3$. The frequencies ($\omega/2\pi$) are: ■, 17.5 MHz; +, 48 MHz; □, 115 MHz; ×, 410 MHz. Stabilisation time per point: 15–20 min. Also see figure 16.

indicates $\omega^2(\Delta T)^{-5}$ to $\omega^2(\Delta T)^{-6}$ behaviour in the steep region, and plateau levels varying approximately proportional to the applied sound frequency $\omega/2\pi$.

For each frequency the measured points within the steep region in the log–log plots were fitted to a flat freely varying background plus a single power law with the amplitude and the exponent, ρ, as free parameters. The exponents, ρ, determined in this way, varied between 4.5 and 6.5, while the amplitudes approximately followed a frequency-squared dependence. However, the data are scattered, and the curve-fitting results were

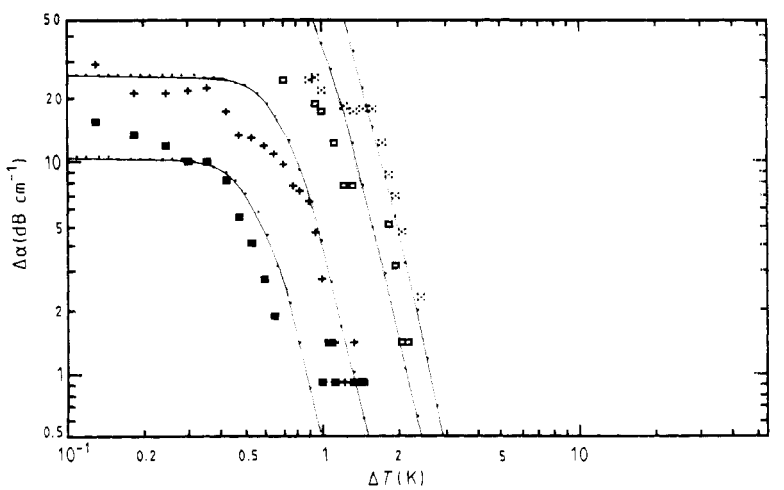

Figure 15. Log–log plots of critical sound attenuation, $\Delta\alpha$, as a function of temperature $\Delta T = T - 103.0$ K for longitudinal waves polarised along the [100] direction in flux-grown $SrTiO_3$. The full curves are given by the scaling forms equations (2) and (4). $\rho = 5.5$ and $\nu z = \rho - \mu = 4.6$. The frequencies ($\omega/2\pi$) are: ■, 20 MHz; +, 60 MHz; □, 225 MHz; ×, 400 MHz.

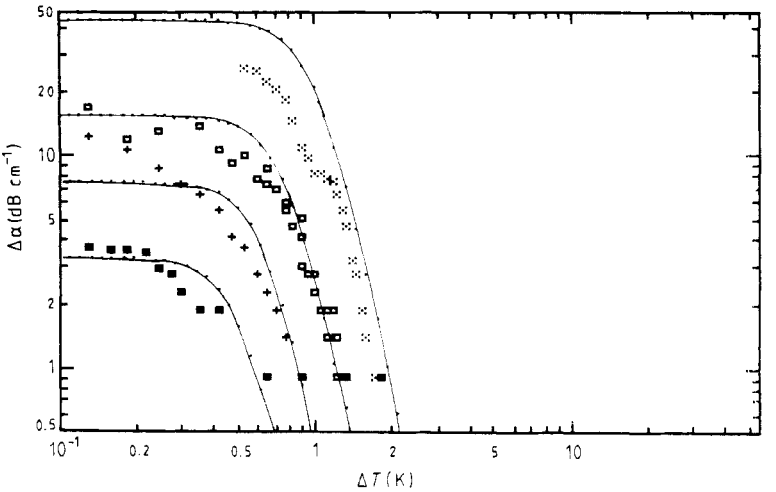

Figure 16. Log–log plots of critical sound attenuation, $\Delta\alpha$, as a function of temperature, $\Delta T = T - T_c$, for transverse waves polarised along the [100] direction for the measurements shown in figure 14. $T_c = 103.0$ K, while the respective backgrounds are identical to the zero level in figure 14 except for the lowest frequency $\omega/2\pi = 17.5$ MHz, where the background is shifted 1 dB cm^{-1} downwards. The full drawn curves are given by the scaling forms in equations (2) and (4). $\rho = 5.5$ and $\nu z = \rho - \mu = 4.6$. The frequencies ($\omega/2\pi$) are: ■, 17.5 MHz; +, 48 MHz; □, 115 MHz; ×, 410 MHz.

not very convincing. Still, it seems clear that the exponent $\rho \sim 5.5 \pm 1$. In the following this value of ρ will be used, and later it will be shown through a Kramers–Kronig analysis that $\rho \sim 5.5$ yields self-consistent results as far as velocity and attenuation *amplitudes* are concerned.

From the theoretical considerations in the preceding theoretical paper, we expect the following asymptotically and causally correct frequency and temperature dependences of critical sound attenuation, when a single-exponent behaviour is assumed:

$$\Delta\alpha = \alpha_0 \omega^2 t^{-\rho} \tag{2}$$

away from T_c and

$$\Delta\alpha = \alpha_0 \tau_0^{-\rho/\nu z} \sin(\pi\mu/2\nu z)\omega^{2-\rho/\nu z} \tag{3}$$

when $\omega\tau \gg 1$, i.e. close to T_c. Here α_0 is the amplitude, $f = \omega/2\pi$ is the sound frequency and $t = (T - T_c)/T_c$ is the reduced temperature. $\tau = \tau_0 t^{-\nu z}$ is the critical relaxation time with amplitude τ_0. The critical exponent $\rho = \mu + \nu z$, where μ is the static sound velocity exponent. The amplitude α_0 is directly proportional to the relaxation time amplitude τ_0. α_0 may be sample dependent since the magnitude of τ_0 possibly depends on concentrations of defects. Thus, α_0/τ_0 is the intrinsic amplitude to be extracted from attenuation measurements.

No static crossover effects are included in this scaling form. From the velocity measurements discussed above we know that a *static* deviation from the $\mu \simeq 0.9$ behaviour occurs close to T_c. Figure 7 shows that for the longitudinal waves this rollover starts at $\Delta T \simeq 0.3$ K and that the measured points at $\Delta T \simeq 0.1$ K are a factor $k \simeq 2$ lower than the line $\mu \simeq 0.9$. In the transverse case, the static deviation from $\mu \simeq 0.9$ starts at $\Delta T \simeq 0.7$ K, giving a lowering of the measurements at 0.1 K by a factor of $k \simeq 2$–3. Note that

except for the lowest frequency ($\omega/2\pi = 17.5$ MHz) for the transverse mode, these effects will not have any influence on the points with $\omega\tau \ll 1$. However, close to T_c, where equation (3) is applied in the data analysis, a static contribution will shift the experimentally determined amplitude downwards, whereas the *frequency dependence will be preserved.* Of course, the latter statement is true only if the velocity saturation does not reveal a crossover to a new type of critical behaviour, which would imply new critical exponents inside the crossover region. This makes it difficult to correct the attenuation data for velocity rollover. The simplest approach to include these effects in the analysis of the sound attenuation results is to replace equation (3) by

$$\Delta\alpha = \frac{\alpha_0 \sin(\frac{1}{2}\pi\mu/\nu z)}{\tau_0^{\rho/\nu z} k}\, \omega^{2-\rho/\nu z} \tag{4}$$

where k is to be estimated from the velocity measurements. The fully drawn curves in figures 15 and 16 are consistent with the scaling forms given in equations (2) and (3). The lower curves in each figure are drawn by inspection as an approximate fit to the data points of the lowest frequency. This determines the amplitudes α_0 and τ_0. The other curves are then completely determined by scaling with the corresponding frequencies.

By plotting $\log y = \log(\Delta\alpha/\alpha_0\omega^2 t^{-\rho})$ against $\log x = \log \omega\tau$, a data collapse on the function $y = (1 + x^{\rho/\nu z})^{-1}$ should be observed, if the scaling forms are correct and if the exponent ρ and μ have been determined correctly.

Such a plot is shown in figure 17. All frequencies for both modes shown in figures 15 and 16 are included. The amplitudes of the scaling functions are the same as those for the fully drawn curves in figures 15 and 16. The scaling plots show the following features clearly.

(i) Away from T_c where $\omega\tau \ll 1$, the data are scattered around the $\omega^2 t^{-5.5}$ behaviour.

(ii) Close to T_c where $\omega\tau \gg 1$, the data behave according to $\omega^{2-\rho/\nu z} t^0$, with $\rho \simeq 5.5$ and $\nu z \simeq 4.6$.

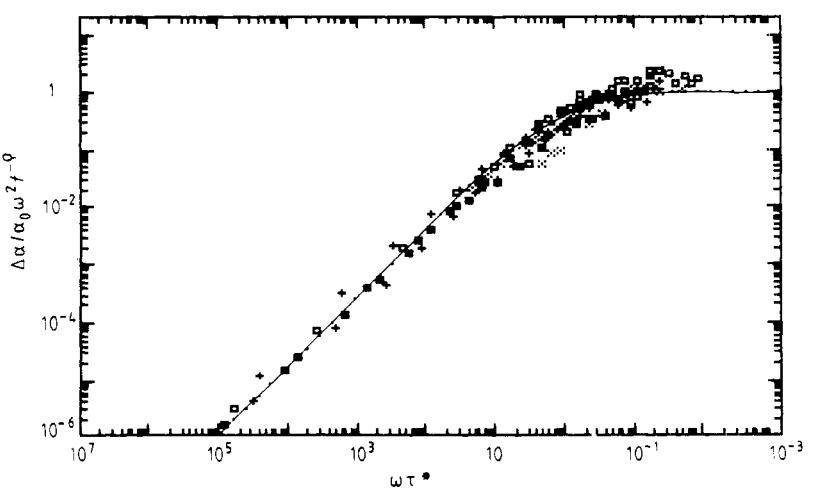

Figure 17. Scaling plot of *all* measured points shown in figures 15 and 16 for flux-grown $SrTiO_3$ with $\boldsymbol{q} \parallel [100]$. Vertical axis: measured attenuation divided by the observed attenuation in the region $\omega\tau \ll 1$. Horizontal axis: $\omega\tau^*$, where $\tau^* = \tau_0^* t^{-\nu z}$, and $\tau_0^{*\rho/\nu z} = k\tau_0^{\rho/\nu z}$ (see text). The full curve is the scaling function $1/[1 + (\omega\tau^*)^{\rho/\nu z}]$, with $\rho = 5.5$ and $\nu z = 4.6$.

(iii) There is a smooth crossover between the asymptotic limits. Most of the data collapse below the phenomenological scaling form $y = 1/(1 + x^{\rho/\nu z})$ in the region $\omega\tau \simeq 1$, indicating that this scaling function is not correct in the intermediate region. One may 'repair' this deviation by choosing a new scaling form: $y = 1/(1 + bx^{\rho/2\nu z} + x^{\rho/\nu z})$, which is also asymptotically correct, but where the amplitude b must be fitted to data in the $x = \omega\tau \sim 1$ region.

(iv) The data scale with frequency consistent with $\rho \simeq 5.5$ and $\nu z = \rho - \mu \simeq 4.6$.

The factor k was introduced above to correct the attenuation data for static rollover. A more proper approach would be to fit a smooth function to the velocity data, and then divide the statics away from the attenuation measurements. This was not tried in the present data analysis, firstly because these effects occur very close to T_c and secondly because of the scattered attenuation data, which implies that one should be happy with self-consistent data analysis which reveals agreements in amplitudes within factors of two.

The results obtained above are summarised in § 3.5. We conclude this section with some comments: in the analysis we have insisted on fitting the data to an ω^2-law away from T_c. The reason for this is that no existing theory predicts anything else. It is impossible to insist on an ω^2 behaviour and low exponents $\rho \sim 1$–3 at the same time. If $\Delta\alpha \sim \omega^2 t^{-\rho}$ in some region away from T_c, then $\rho \sim 4.5$–6.5 is the only possibility. It is also clear that the steep $\rho \simeq 5.5$ behaviour can not be avoided either by changes of ± 1 dB cm^{-1} in the background levels, or by shifts in T_c within the range 103.0 ± 0.1 K.

3.4. Sound attenuation measurements in Verneuil-grown $SrTiO_3$

It has been argued that the large amounts of macroscopic strains in the Verneuil-grown sample, observed in the microscope, were revealed experimentally in the velocity

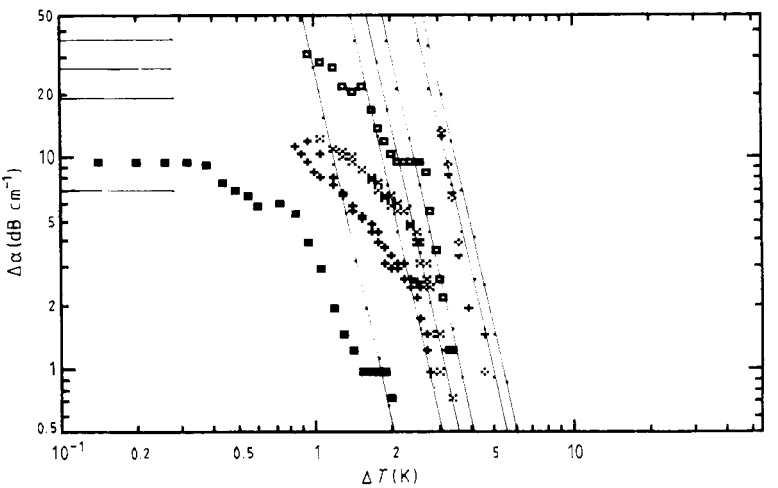

Figure 18. Critical sound attenuation, $\Delta\alpha$, as a function of temperature, T, for longitudinal waves along the [100] direction in Verneuil-grown $SrTiO_3$. Phonon echo (E) and conventional pulse reflection (R) measurements are shown. Stabilisation time per point was about 15 min. $T_c = 104.9$ K. The echoes (E) are measured twice. The straight lines are drawn according to a $\omega^2 t^{-5.5}$ behaviour, while the 'saturation' levels follow an $\omega^{(2-5.5/4.6)}$ law. The frequencies ($\omega/2\pi$) are: ■, 33 MHz (R); +, 108 MHz (E); ×, 165 MHz (E); □, 240 MHz (R); ◇, 530 MHz (R); ⊤, 670 MHz (R).

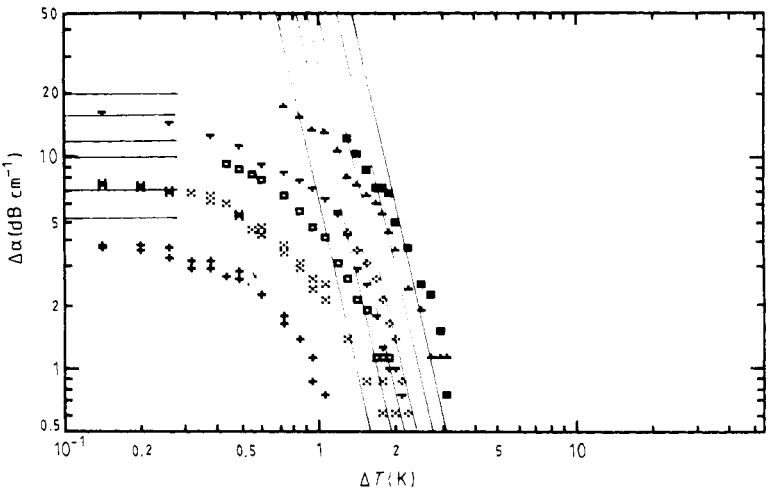

Figure 19. Critical sound attenuation, $\Delta\alpha$, as a function of temperature, T, for longitudinal waves along the [111] direction in Verneuil-grown $SrTiO_3$. Both phonon echo (E) and reflection (R) measurements are shown. The stabilisation time per point was 15–20 min. The two lowest frequencies represent two different series of measurements each. The lines and the 'saturation' levels are consistent with $\rho = 5.5$ and $\nu z = 4.6$ (see text). The frequencies ($\omega/2\pi$) are: +, 110 MHz (E); ×, 170 MHz (E); □, 250 MHz (E); ◇, ⊤, 325 MHz (E, R); ⊥, 470 MHz (R); ■, 630 MHz (R).

experiments. We now turn to a discussion of the attenuation measurements on this sample, as summarised in the figures 18–21. There is little doubt that the scatter in the measured points is caused at least partly by the macroscopic defects. As expected the phonon echo data (E) are less scattered than the reflection data (R).

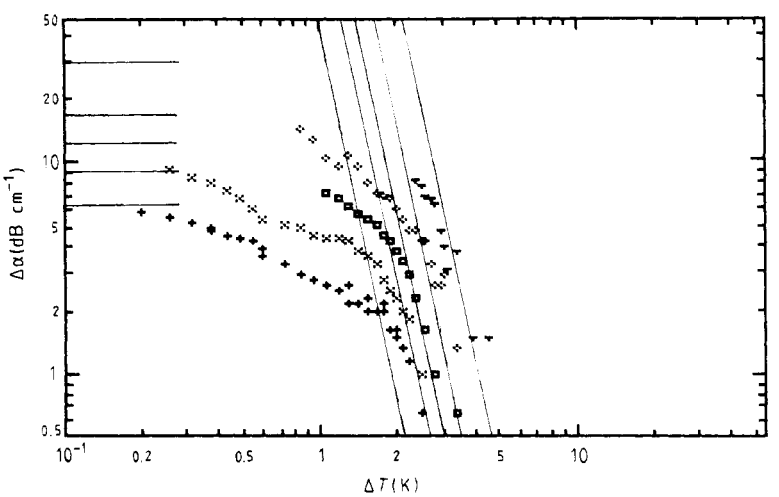

Figure 20. Critical sound attenuation, $\Delta\alpha$, as a function of temperature, $\Delta T = T - T_c$, for longitudinal sound along the [110] direction in Verneuil-grown $SrTiO_3$. $T_c = 104.9$ K. The echo (E) at 105 MHz is measured twice. The steep lines and the 'saturation' levels are consistent with $\rho = 5.5$ and $\nu z = 4.6$ (see text). The frequencies ($\omega/2\pi$) are: +, 105 MHz (E); ×, 165 MHz (E); □, 230 MHz (E); ◇, 350 MHz (R); ⊤, 670 MHz (R).

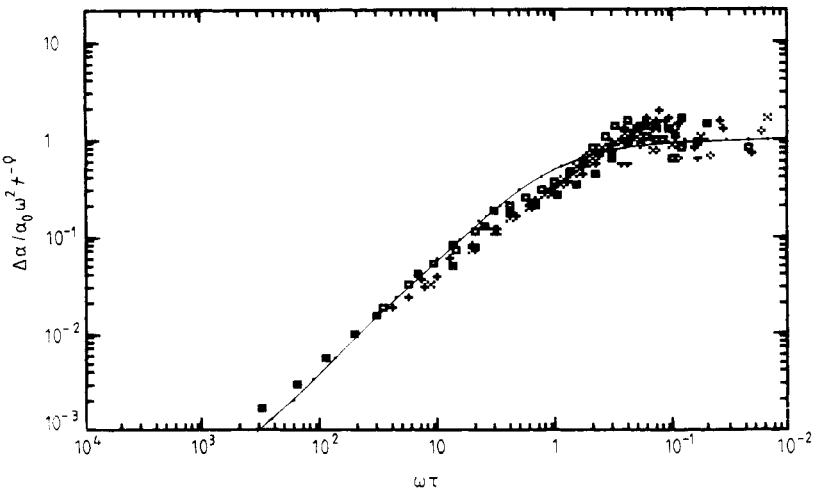

Figure 21. Dynamic scaling plot for the longitudinal [100] mode (see figure 18) for Verneuil-grown $SrTiO_3$. For explanation of symbols see the text. The full curve is the scaling function $y = 1/(1 + x^{\rho/\nu z})$. The frequencies $(\omega/2\pi)$ are: ■, 33 MHz (R); +, 108 MHz (E); ×, 165 MHz (E); □, 240 MHz (R); ◇, 530 MHz (R); ⊤, 670 MHz (R).

No trustworthy determination of T_c could be obtained from any of these measurements. A maximum in the critical attenuation similar to figure 13 at 104 ± 0.1 K was measured at one low frequency ($\omega/2\pi = 16$ MHz), for the transverse polarised [100] mode. The maximum did not reproduce, however, when the measurement was repeated some weeks later. Thus, as for the velocity measurements, we will use the value of T_c determined from heat capacity measurements by Stokka and Fossheim (1982), i.e. $T_c = 104.9 \pm 0.1$ K. The background levels of attenuation in these cases are believed to be determined within ± 2 dB, i.e. within ± 0.5 dB cm^{-1} in the plotted figures (sample lengths: 2–3 cm).

As for the velocity experiments, four different sound modes were investigated. The resulting log–log plots of the critical attenuation, $\Delta\alpha$, against temperature, $\Delta T = T - 104.9$ K, are shown in the figures 18–20. The stabilisation time per measured point was 15–20 min. The straight lines in the figures 18–20 are drawn according to a $\omega^2 t^{-\rho}$ behaviour, with $\rho = 5.5$ while the indicated 'saturation' levels near T_c follow an $\omega^{2-\rho/\nu z}$ law, with $\rho/\nu z = 5.5/4.6 = 1.19$. The choice of exponents is of course motivated by the results obtained on the flux-grown sample. The qualitative similarities between the behaviours in the two samples are striking: a steep increase in the attenuation on approaching T_c from above, followed by a rollover approaching a pleateau near T_c. We will refer to this loosely as the dynamic levelling-off. Also for the Verneuil sample it is impossible to fulfil an $\omega^2 t^{-\rho}$ law, unless $\rho \sim 5.5$. From figure 11 we can also see that the static rollover starts at $T_c + 0.8$ K. From figure 18 it follows that except for the lowest frequency, $\omega/2\pi = 33$ MHz, all data of the longitudinal polarised [100] mode are unaffected by the velocity rollover. Therefore, this mode is the best candidate for determining the amplitude of the relaxational time in this sample, whereas the [111] mode should be the most difficult one. Figure 21 represents a dynamic scaling plot of data plotted in figure 18.

Due to the large uncertainties in the data, scaling plots should not be taken as evidence, but merely as indications that even these data scale with the frequency accord-

ing to $\rho \sim 5.5$ and $\nu z \sim 4.6$. Note however the *difference* in amplitudes between the two samples in the steep $\omega\tau \ll 1$ region. A simple comparison between the respective longitudinally polarised [100] modes yields, after frequency scaling, an amplitude higher by a factor of ten for the Verneuil-grown sample than for the flux-grown one. Since the amplitudes are directly proportional to the relaxation time amplitude τ_0 when $\omega\tau \ll 1$, we may conclude that the measured relaxation time amplitude is smaller by approximately a factor of ten in the flux-grown than in the Verneuil-grown sample. We will return to this observation below.

3.5. *Summary of results*

Above results from ultrasonic measurements mainly at $T > T_c$ on two different types of $SrTiO_3$ samples were presented. Except for the magnitudes of the measured relaxation time amplitudes τ_0, both qualitative and quantitative results were similar in the two samples. The most accurate and therefore also most reliable results emerged from the velocity measurements on the flux-grown sample. In this case *a first-order character* of the transition was revealed. The sound velocity exponent was determined to be

$$\mu = 0.89 \pm 0.06.$$

Due to large amounts of macroscopic inhomogeneities in the Verneuil-grown sample, no accurate determination of the exponent μ was possible. However, simple inspection indicates a single-exponent behaviour with $\mu \simeq 0.9$ for all the modes also investigated in this case. For both samples a rollover of the velocity anomaly was observed on approaching T_c, while at high temperatures, $\Delta T > 15$ K, a behaviour steeper than $\Delta T^{-0.9}$ was measured. No frequency dependence of the velocity could be resolved from measurements on the flux-grown sample at any temperature above T_c. The measurements give no reason for claiming significantly different singularity amplitudes of sound velocity in the two samples (see table 1).

The sound attenuation data from both samples are somewhat scattered. However, the qualitative behaviour is clear: a steep increase followed by a saturation on approaching T_c from above. If a frequency-squared behaviour is insisted on in the steep region, then the exponent

$$\rho \simeq 5.5 \pm 1$$

is the only reasonable choice for both samples. From the amplitude and frequency dependences of the saturation levels, one can estimate the amplitude, τ_0, of a relaxation time $\tau = \tau_0 t^{-\nu z}$, where $\nu z = \rho - \mu$. Due to the 'saturation' of the velocity on approaching T_c, there are uncertainties in the magnitudes of τ_0 in the two samples. The reason for this is that one cannot tell whether the latter saturation is of dynamic origin, whether it is pure static and connected to smearing of T_c or the first-order character of the transition, or if it represents crossover to another universality class.

The attenuation measurements were found to scale with frequency according to the phenomenological expressions cited above. Table 1 gives a summary of the measured sound velocity coefficients, while the amplitudes of the critical parts of the attenuation are summarised in table 2.

Some comments on table 2: the amplitudes $A = \Delta\alpha(\Delta T = 1\ \mathrm{K})/\omega^2$ are determined from the various $\omega\tau \ll 1$ behaviours, while the τ_0 are given by the amplitudes of 'saturation' levels as described in the preceding sections. A static contribution to the saturation will result in an overestimation of τ_0.

Table 1. Summary of results obtained from velocity measurements on the two $SrTiO_3$ samples. The sound mode is denoted by L*hkl* or T*hkl*, where L and T mean longitudinal and transverse polarisation respectively, whereas *hkl* denote the direction of wave propagation. $\Delta v(\Delta T = 1\ \mathrm{K})$ is the amplitude of the critical part of the velocity at $\Delta T = 1$ K. $k(\Delta T = 0.1\ \mathrm{K})$ is the factor by which the data points are lowered compared with the $\mu = 0.9$ line at $\Delta T = 0.1$ K, while ΔT_r is the temperature where the velocity rollover towards T_c starts. Note that the background levels may differ by an amount $\Delta A_1 = nv^2/(2l\omega/2\pi)\ \mathrm{m\,s^{-1}}$, where v is the total velocity, l is the length of the sample (measured in metres) and $n = 1, 2, 3, \ldots$. This is due to the uncertainty connected with overlapping of identical cycles of the pulses. This explains the discrepancy between the measured background levels in the two samples.

Sample	Sound mode L, longitudinal T, transverse	Frequency $\omega/2\pi$ (MHz)	Background ($\mathrm{m\,s^{-1}}$) $A_1 - A_2T$ T = Temperature (K)	$\Delta v(\Delta T = 1\ \mathrm{K})$ ($\mathrm{m\,s^{-1}}$)	$k(\Delta T = 0.1\ \mathrm{K})$	ΔT_r (K)
Flux-grown	L100	20	7861.46–0.7774 T	275	2	0.3
		17.5				
	T100	80	4875.40–0.2622 T	62	2–3	0.7
Verneuil-grown	L100	33	8109.40–09622 T	300	4	0.8–1
	L111	30	8210.00–0.6237 T	95	4	0.8–1
	L110	32	8283.74–0.6946 T	220	4	0.8–1
	T100	16	4918.21–0.2034 T	60–100	4	0.8–1

Table 2. Summary of results obtained from attentuation measurements. $\Delta\alpha(\Delta T = 1\ \mathrm{K})/\omega^2$ are the estimated amplitudes at $\Delta T = 1$ K. τ_0 are the estimated relaxation time amplitudes, while τ_0^* is the sample quantity, but the uncertainties due to the velocity saturation are incorporated. $\Delta\alpha(\Delta T = 1\ \mathrm{K})/\omega^2\tau_0$ are the intrinsic attenuation amplitudes. The attenuation amplitudes are believed to be determined within factors of two.

Sample	Sound mode	$\Delta\alpha(\Delta T = 1\ \mathrm{K})/\omega^2$ ($\mathrm{dB\,cm^{-1}\,s^2}$)	τ_0(s)	τ_0^*(s)	$\Delta\alpha(\Delta T = 1\ \mathrm{K})/\omega^2\tau_0^*$ ($\mathrm{dB\,cm^{-1}\,s}$)
Flux-grown	L100	3.3×10^{17}	3.7×10^{19}	$(2.9 \pm 0.8) \times 10^{19}$	150
	T100	5.7×10^{-18}	2.0×10^{-19}	$(1.4 \pm 0.8) \times 10^{19}$	27
Verneuil-grown	L100	5.6×10^{16}	7.9×10^{-18}	$(6 \pm 2) \times 10^{-18}$	140
	L111	2.1×10^{-17}	1.3×10^{-18}		
	L110	1.7×10^{-16}	5.9×10^{18}	$(4 \pm 2) \times 10^{18}$	43

Since A/τ_0 is an intrinsic quantity, this ratio ought to be the same in the two samples. This would require that $\tau_0 \simeq 2.2 \times 10^{-19}$ and 4×10^{-18} s in the flux-grown and Verneuil-grown samples respectively.

Since $\tau = \tau_0 t^{-\nu z}$, we obtain with $\nu z = 4.6$:

$$\tau(\Delta T = 1\ \mathrm{K}) \simeq 4.0 \times 10^{-10}\ \mathrm{s} \qquad \text{flux-grown sample}$$

and

$$\tau(\Delta T = 1\ \mathrm{K}) \simeq 7.9 \times 10^{-9}\ \mathrm{s} \qquad \text{Verneuil-grown sample.}$$

The T100 measurements on the Verneuil-grown sample are not analysed at all due to the scatter in the data. The L111 data (also those with $\omega\tau \ll 1$) are situated within the static rollover region, which makes it difficult to estimate both A and τ_0 in this case.

4. Discussion

The self-consistency of the results presented in the previous sections can be tested in two ways. Firstly, the amplitudes of the different sound modes are connected through symmetry relations. Secondly, the amplitudes of velocity and attenuation for the same mode are connected through Kramers–Kronig relations (causality requirements). Both symmetry and causality have been taken into account in the phenomenological predictions presented in § 8 in the theoretical paper. The symmetry relations will be tested on the velocity amplitudes, because these are determined more accurately than the attenuation amplitudes. We will assume that the anomaly of the non-symmetry breaking elastic modulus, C_a, is negligible. The analysis below verifies this assumption. Symmetry predicts the following relations:

$$\Delta v_{\mathrm{T100}}/v^0_{\mathrm{T100}} = \tfrac{3}{4}\Delta v_{\mathrm{L111}}/v^0_{\mathrm{L111}} \tag{5}$$

$$\Delta v_{\mathrm{L110}}/v^0_{\mathrm{L110}} = \Delta v_{\mathrm{T100}}/v^0_{\mathrm{T100}} + \tfrac{1}{4}\Delta v_{\mathrm{L100}}/v^0_{\mathrm{L100}} \tag{6}$$

where the Δv and the v^0 are the anomalies and the background values respectively. The results inserted from table 1 are summarised in table 3.

The Kramers–Kronig integration performed in the preceding theoretical paper

Table 3. Check on the symmetry relations equations (5) and (6) for the velocity amplitudes. Results are inserted from table 1. (L100 and T100: flux-grown sample, L111 and L110: Verneuil-grown sample). The result verifies equations (5) and (6), and therefore also the validity of neglecting the non-symmetry-breaking contribution, which would contribute equally to the longitudinal modes.

$\dfrac{\Delta v_{\mathrm{L100}}}{v^0_{\mathrm{L100}}}$	3.4×10^{-2}		
$\dfrac{\Delta v_{\mathrm{L111}}}{v^0_{\mathrm{L111}}}$	1.2×10^{-2}		
$\dfrac{\Delta v_{\mathrm{L110}}}{v^0_{\mathrm{L110}}}$	2.7×10^{-2}	$\dfrac{\Delta v_{\mathrm{T100}}}{v^0_{\mathrm{T100}}} + \dfrac{1}{4}\dfrac{\Delta v_{\mathrm{L100}}}{v^0_{\mathrm{L100}}}$	2.2×10^{-2}
$\dfrac{\Delta v_{\mathrm{T100}}}{v^0_{\mathrm{T100}}}$	1.3×10^{-2}	$\dfrac{3}{4}\dfrac{\Delta v_{\mathrm{L111}}}{v^0_{\mathrm{L111}}}$	0.9×10^{-2}

(Fossum 1984) predicts for each sound mode:

$$\Delta v(\Delta T = 1\,\mathrm{K}) = \frac{\nu z}{\mu} v_0^2 \frac{\Delta\alpha(\Delta T = 1\,\mathrm{K})}{\omega^2 \tau(\Delta T = 1\,\mathrm{K})} \frac{100}{8.68} \tag{7}$$

where v_0 is the background velocity, $\Delta v(\Delta T = 1\,\mathrm{K})$ is inserted in units of $\mathrm{m\,s^{-1}}$, while $\Delta\alpha(\Delta T = 1\,\mathrm{K})/\omega^2$ is inserted in units of $\mathrm{dB\,cm^{-1}\,s^2}$. The factor 100/8.68 converts $\mathrm{dB\,cm^{-1}}$ to $\mathrm{m^{-1}}$. The results for the different modes are summarised in table 4. For both samples, satisfactory results are obtained only for the longitudinally polarised [100] mode, while the least satisfactory result is the one for the L111 mode. This is not surprising for the reasons discussed in the preceding paragraph. In § 3.5 we saw that the relaxation time amplitude was approximately one order of magnitude larger in the Verneuil-grown sample than in the flux-grown one. It is important to stress that this conclusion does not depend on the analysis of the dynamic rollover of the attenuation data alone. It is only necessary to compare the attenuation amplitudes of the two samples in the region $\omega\tau \ll 1$, to convince oneself about the difference in the τ_0. We have, however, seen that there are two independent ways of estimating the amplitudes τ_0, namely: (i) from the attenuation rollover and (ii) from a Kramers–Kronig comparison in the regime $\omega\tau \ll 1$ via equation (7).

We have arrived at conclusions concerning both what could be universal and non-universal behaviours in the two $SrTiO_3$ samples investigated. The possible static and dynamic universal properties are contained in the exponents $\mu \simeq 0.89$ and $\nu z \simeq 4.6$. Non-universal properties determine amplitudes, among which the relaxation time amplitude, τ_0, is of particular interest.

The data analysis has revealed single-exponent-like behaviour both for the velocity and the attenuation. However, due to the rollover behaviour of both quantities on approaching T_c, we can not be absolutely sure that the true asymptotic behaviour has really been revealed. It could very well be that the asymptotic behaviour is hidden inside the rollover region, and that the exponents we have measured are effective ones, where correction to scaling terms should be included in the analysis. It could also be that the observed exponents describe some preasymptotic behaviour connected to Hamiltonian flow close to an unstable or inaccessible fixed point, or that our exponents are dominated by defects. We use the term exponents for μ and νz although they might not be *critical* exponents, merely effective ones describing some precritical behaviour.

Since there is no way in which the measurements can tell us if something interesting

Table 4. Summary of the Kramers–Kronig analysis. $\Delta v(\Delta T = 1\,\mathrm{K})$, $\Delta\alpha/\omega^2(\Delta T = 1\,\mathrm{K})$ and $\tau(\Delta T = 1\,\mathrm{K})$ are the amplitudes of the velocity, attenuation and relaxation time respectively at $\Delta T = 1\,\mathrm{K}$. $\rho = 5.5$ and $\mu = 0.9$. v_0 is the background velocity. The factor 100/8.68 converts $\mathrm{dB\,cm^{-1}}$ to $\mathrm{m^{-1}}$. The amplitudes are inserted from tables 1 and 2 and from the text.

Sample	Mode	$\Delta v(\Delta T = 1\,\mathrm{K})$ ($\mathrm{m\,s^{-1}}$)	$\frac{\nu z}{\mu} v_0^2 \frac{\Delta\alpha(\Delta T = 1\,\mathrm{K})}{\omega^2\tau(\Delta T = 1\,\mathrm{K})} \frac{100}{8.68}$ ($\mathrm{m\,s^{-1}}$)
Flux-grown	L100	275	320
	T100	62	20
Verneuil-grown	L100	300	280
	L111	95	11
	L110	220	87

happens within the static and dynamic rollover regions, we are forced to discuss the exponents obtained outside these regions. It should be noted that the temperature at which the velocity rollover starts, is sample dependent, and therefore at least partly a non-universal feature. The most accurate data, namely the ones for the velocity of the longitudinally polarised [100] mode in the flux-grown sample, showed straight-line behaviour in the log–log plot over one and a half decades. For this reason we do not believe that correction to scaling terms that vary strongly with temperature should be included as far as the static behaviour is concerned.

We have argued that contributions from the non-symmetry-breaking mode are negligible (also see Murata 1976). Thus, we expect $\mu = \alpha + 2(\varphi - 1)$, where α is the heat capacity exponent, and φ is the symmetry-breaking crossover exponent describing the curvature of the stress–temperature phase boundary in the vicinity of the zero-external-stress critical point.

In mean-field theory $\varphi = 1$, while $\alpha = 2 - d/2$ in the gaussian approximation (Ma 1976), i.e. $\mu = 0.5$ for $d = 3$ and $\mu = 1$ for $d = 2$, in this case. Thus the measured exponent $\mu \simeq 0.9$ is close to, but significantly smaller than, the two-dimensional classical one.

If $SrTiO_3$ belongs to the isotropic $d = 3$ Heisenberg universality class one expects $\mu = \alpha + 2(\varphi - 1) \simeq 0.4$ (Aharony and Bruce 1974), since the non-classical crossover exponents that are expected to come into play in $SrTiO_3$ are the ones describing crossover away from isotropic Heisenberg or cubic behaviour to XY or Ising behaviour. Theoretically the isotropic crossover exponent is determined to be $\varphi = 1.25 \pm 0.015$ (Pfeuty *et al* 1974), while Aharony (1974) has calculated the cubic one as $\varphi = 1.23$ for $n = d = 3$. Stokka and Fossheim (1982) determined phase diagrams from heat capacity measurements. They found $\varphi = 1.27 \pm 0.06$ in $SrTiO_3$, while Müller *et al* (1984) have reported $\varphi = 1.31 \pm 0.07$ from EPR experiments on $LaAlO_3$.

Thus, the quantity $2(\varphi - 1) \sim 0.46$–0.52 theoretically, while $2(\varphi - 1) \sim 0.42$–0.76 from experiments. To explain $\mu = 0.89 \pm 0.06$ one then needs an exponent $\alpha > 0$. Both the Heisenberg and the cubic fixed point have a small negative value of α (Fisher 1974). We must therefore conclude that neither the isotropic nor the cubic fixed-point exponents can explain our most reliable result, namely $\mu = 0.89 \pm 0.06$.

Inserting the result of Stokka and Fossheim, $\varphi = 1.27 \pm 0.06$, into $\mu = \alpha + 2(\varphi - 1)$, we obtain $\alpha = 0.34 \pm 0.18$. No determination of α in unstressed $SrTiO_3$ exists. Hatta *et al* (1977) found $\alpha = 0.125$ corresponding to Ising behaviour in uniaxially stressed $SrTiO_3$. To our knowledge, the only intrinsic heat capacity exponent which agrees with this result is the tricritical one, $\alpha_t = 0.5$. We will return to this possibility below.

Here we proceed by introducing non-asymptotic or non-critical behaviour consistent with $\mu \sim 0.9$. Schwabl (1974) and Nattermann (1976) have suggested a possible crossover to $d = 2$ behaviour *away* from T_c ('pancake'-like correlations). At ordinary critical points, $\alpha \simeq 0$ also for $d = 2$, while $\nu = 1$ is obtained in the $d = 2$ Ising model. Thus $\varphi \simeq 1.45$ and $z > 4.6$ is needed. No theory predicts the latter, whereas simple insertion of $n = 3$, $d = 2$ into the expression for the isotropic crossover exponent (see, for example, Fisher (1974)), gives $\varphi = 1.38$, which is close to the result required. However, it is unclear whether it has meaning to use the calculated expression for φ in this case, since there is no long-range order in an isotropic model with $n = 2$ or 3 and $d = 2$ (Mermin and Wagner 1966).

Above we mentioned that $\mu \sim 0.9$ is close to its $d = 2$ gaussian value $\mu = 1$. In fact, Courtens (1976) has explained birefringence measurements in the high-temperature

phase of $SrTiO_3$ in terms of a two-dimensional Ornstein–Zernike approach. An argument against the existence of two-dimensional correlations in $SrTiO_3$ is found by comparing with results obtained on $KMnF_3$ (Holt and Fossheim 1981). $KMnF_3$ does not behave according to $d = 2$, and due to a dispersion anisotropy term in the model Hamiltonian, one expects the behaviour of $KMnF_3$ to be more two dimensional than that of $SrTiO_3$ (Natterman and Trimper 1975, Natterman 1976).

We will now turn to a discussion of non-intrinsic behaviour. Here there are several possibilities, including macroscopic strains or local disorder due to impurities or other defects. The present experiments show that we can exclude random internal macroscopic strains as an explanation of the observed exponents. The reason for this is the different properties of the two samples. Strains were visible under crossed polarisers only in the Verneuil-grown crystal. However, both samples gave $\mu \sim 0.9$ (and $\nu z \sim 4.6$).

The two samples are very different as far as colour and macroscopic strains are concerned and these arise from different sources. However, the samples could contain the same kind of microscopic defects by accident. Levanyuk *et al* (1979) have considered the role of defects as nucleation centres close to phase transitions. They arrived at heat capacity exponents $\alpha \simeq 1.4$–1.5, and sound attenuation exponents $\rho \simeq 2.5$–2.7 for $d = 3$ short-range systems, whereas $\alpha \simeq 1.0$–1.2 and $\rho \simeq 3$–4.5 for $d = 2$. The mean-field results of Levanyuk *et al* (1979) are $\alpha = 1.5$ and $\rho = 2.5$. Only the two-dimensional values are comparable with *our* results. Höchli and Bruce (1980), who reported $\mu \simeq 1.5$ from acoustic resonance measurements of elastic compliances in $SrTiO_3$, interpreted their result as $d = 3$ defect dominated.

Bäuerle and Rehwald (1978) measured sound velocity in semiconducting $SrTiO_3$ (probably Verneuil-grown). The transition temperature was lower in samples which had been reduced in hydrogen and was increased in Nb-doped samples. The critical exponent in the pure samples was determined to be $\mu \sim 0.76$ ($T_c = 104.7 \pm 0.1$ K), while it increased as a function of increasing carrier concentration to $\mu \sim 1.6$ ($T_c = 97.0 \pm 2$ and 107.6 ± 0.4 K respectively) for the largest concentrations. An exponent $\mu = 0.84$ and $T_c = 97.6 \pm 0.1$ K was measured in a sample which was reduced in hydrogen for 10 h. No attenuation measurements have been reported on semiconducting samples.

Although $T_c \sim 103$–105 K in both our samples, and although the present crystals have not been exposed to the same kind of *treatment* as far as impurities are concerned, it seems that we cannot completely exclude an explanation of our results for exponents in terms of defect concentrations as a possibility.

As we know, and will return to below, there is a difference between the relaxation time amplitudes of the two samples. *This* difference is probably due to different defect concentrations.

We now return to the possibility of tricritical behaviour, which was mentioned above. This, in our view, represents the most interesting explanation. Our measurements on the flux-grown sample indicate a weakly first-order character of the transition. If this really is the case, then unstressed $SrTiO_3$ could be close to a tricritical point, since the measurements of Stokka and Fossheim (1982) show that the transition is second order if an infinitesimal pressure is applied along the [100] direction.

The suggestion that well annealed $SrTiO_3$ possesses a first-order transition which is close to tricriticality has been put forward by Müller (1982), in order to explain EPR measurements by Müller and Berlinger (1982). They performed experiments with compression and tension along the [111] direction. The resulting phase diagram was

inconsistent with predictions by Bruce and Aharony (1975) based upon the assumption that the unstressed crystal showed a second-order transition. Müller and Berlinger's observations could be explained from a phase diagram calculated by Blankschtein and Mukamel (1982), provided that the unstressed $SrTiO_3$ sample was weakly first order.

Neutron scattering experiments on flux-grown $SrTiO_3$ (unstressed) by Okazaki *et al* (1983) revealed a first-order-like transition, which in that case was explained as residual strains of the low-temperature phase. In the present results on the flux-grown sample the hysteresis (see figures 5 and 6) can be explained in this manner, but not the observed steps at T_c as a function of decreasing temperature. Remember that in the measurement shown in figure 5, the sample has been cooled slowly from room temperature. It had never been cooled below T_c before. It should in this context also be mentioned that unpublished results by Berre (1983), who measured sound velocity in Verneuil-grown $SrTiO_3$ under relatively large [111] compression, revealed larger but qualitatively similar *steps* at T_c. Thus under conditions where the transition clearly is first order, the qualitative first-order features of the present experiments *are* observed.

Rehwald (1977) measured sound velocity exponents in $SrTiO_3$ under stress (both uniaxial [100] and biaxial [100], [010]), i.e. the same type of experiment as the one of Stokka and Fossheim (1982). Rehwald found $\mu = 0.60$–0.71 in the unstressed samples, while $\mu \simeq 0.40$–0.60 at the largest applied stresses. The transition temperature was shifted upwards as expected from a theoretical phase diagram (Aharony and Blankschtein 1984). The decreasing value of $\mu = \alpha + 2(\varphi - 1)$ can be interpreted as a decrease either of α or of φ or maybe of both. The experiments of Stokka and Fossheim (1982) revealed *no* decrease of φ for stresses corresponding to those of Rehwald (1977). Thus we must assume that the decreasing value of μ as a function of increasing pressure reflects a decrease of α from $\alpha \simeq 0.5$ to lower values, i.e. Rehwalds experiments could be interpreted as moving away from tricriticality.

What about dynamics in this context? Our measurements may be interpreted as giving $\nu z \sim 4.6 \pm 1$. νz may be an effective exponent. Note also that the dynamic asymptotic region may be different from the static one, that is one could imagine that dynamic correction to scaling terms are important although static asymptotics is fulfilled. From theory $z_t = 3$ at tricriticality (Dohm 1984), while $\nu_t = \frac{1}{2}$ (Blume 1974). Although z_t is larger than 'ordinary' $z = 2$, $\nu_t z_t = 1.5$ does not agree with that estimated from our, admittedly scattered, attenuation data.

Few experiments on ultrasound attenuation close to tricritical points are found in the literature. We mention two examples.

Rehwald and Lang (1975) measured velocity and attenuation in $Sn_xGe_{1-x}Te$, for different values of x. This crystal is known to possess a tricritical point for $x_t = 0.73$ (second order for $x > x_t$, first order for $x < x_t$) (Clarke 1978). Rehwald and Lang's results revealed logarithmic divergence of the sound velocity in these samples, whereas the attenuation exponents were found to increase dramatically in samples close to tricriticality. For $x = 0.75$, $\rho \sim 3.4$–4.5 was found, while $\rho \sim 0.7$–1.1 for $x = 0.91$. Rehwald and Lang were not able to explain their large exponents.

Another example to be found in the literature is the work by Hikita *et al* (1982), who measured velocity and attenuation in $(NH_4)_2BeF_4$ (AFB) as a function of hydrostatic pressure. A doubling of the exponent ρ at one intermediate value of the pressure was interpreted as passing through 'some kind of multicritical point'.

Of course we have mentioned these two particular examples because they show features similar to our results. Another system which is believed to possess a tricritical

point is NH_4Cl. No large sound attenuation exponents are observed in the vicinity of this point (Leung *et al* 1979). However, tricritical behaviour is the only explanation in terms of an asymptotic universality class we are able to offer. The tricritical point in NH_4Cl is an ordinary one, i.e. a so called gaussian tricritical point. The multicritical point in question in the unstressed perovskites need not be a gaussian tricritical point, but it might be a critical end point, where the phase transition also changes from first to second order. There is experimental support to conclude that unstressed $SrTiO_3$ (Müller 1982) is closer to a critical end point than unstressed $KMnF_3$ or $RbCaF_3$ (Fossheim 1984, Buzaré *et al* 1984). To our knowledge there exists no predictions for exponents close to critical end points.

We now turn to the amplitude of the relaxation time, τ_0, which was determined as $\tau^{-1}(\Delta T = 1\,\mathrm{K}) = 2.5 \times 10^3\,\mathrm{MHz}$ for the flux-grown sample, while $\tau^{-1}(\Delta T = 1\,\mathrm{K}) = 120\,\mathrm{MHz}$ in the Verneuil-grown one. At $\Delta T = 0.1\,\mathrm{K}$ the inverse times are $\tau^{-1}(\Delta T = 0.1\,\mathrm{K}) = 0.02$–$0.2\,\mathrm{MHz}$ and $\tau^{-1}(\Delta T = 0.1\,\mathrm{K}) = 0.001$–$0.01\,\mathrm{MHz}$ respectively. We interpret the order-of-magnitude difference between the two times, as being due to defects. It seems that the defect(s) in question do not affect the exponents qualitatively, but do determine the timescale.

It is, of course, tempting to suggest that the important defects as far as the two different timescales are concerned are the macroscopic strains. These are not present in the flux-grown sample, which means that clusters (which may be defect induced) will have shorter lifetimes in this sample than in the Verneuil-grown one, where macroscopic strains indeed are present.

However, the same effect could also be obtained from *different* amounts in the two samples of randomly (or clustered) distributed microscopic defects. This would mean larger amounts of microscopic defects in the flux-grown samples than in the Verneuil-grown one. The presence of such defects in rather high concentration is evident in these crystals since they have a homogeneous brownish colour. These crystals are different from the Verneuil-grown ones has been clearly demonstrated in EPR work by Müller and co-workers. Very strong microwave absorption was observed in these crystals (Müller 1982). In the present experiments, slow dynamics was observed in the sound velocity below T_c in the flux-grown sample, in agreement with observations made by Okazaki *et al* (1983) and D'iorio *et al* (1983).

We have already connected the measured relaxation times to cluster dynamics and to defects, which means that the cluster dynamics in question would not be a purely intrinsic one. One could also suggest a *completely* extrinsic origin of the observed dynamics, namely that the timescales are set by hopping of defects between different sites (Halperin and Varma 1976).

The magnitudes of the relaxation times are comparable with the inverse width, τ_c, of the central peak in $SrTiO_3$. Neutron scattering studies (Töpler *et al* 1977) gave $\tau_c^{-1} = 20\,\mathrm{MHz}$ as an upper limit, while Lyons and Fleury (1977) were able to suggest $\tau_c^{-1} = 300\,\mathrm{MHz}$ as the upper limit. The EPR studies made by Reiter *et al* (1980) *gave* $\tau_c^{-1} < 6\,\mathrm{MHz}$. Our results are comparable with the cited ones, i.e. our relaxation times can very well be connected to the width of the central peak in $SrTiO_3$.

In principle there is of course an additional possibility, namely that our relaxation time is connected to the soft-phonon timescales. At $\Delta T \simeq 1\,\mathrm{K}$ the soft-phonon frequency $\omega_\infty > 1.3 \times 10^5\,\mathrm{MHz}$, while the width of the overdamped soft phonon $\omega_\infty^2/2\Gamma > 4.2 \times 10^4\,\mathrm{MHz}$, as determined from neutron scattering measurements made by Shapiro *et al* (1972). The soft-phonon timescales are definitely shorter than (and are therefore probably not connected to) our relaxation times.

There still seems to be a correspondence between the degree of overdamping of the soft phonon and the appearance of attenuation anomalies as a function of temperature. In $SrTiO_3$ the soft mode is underdamped until a few degrees above T_C, while in $KMnF_3$ the soft mode is already overdamped 40 K above the 186 K transition. The sound attenuation anomaly in $SrTiO_3$ grows up approximately at the temperature at which the soft-mode becomes overdamped, while in $KMnF_3$, the attenuation anomaly starts growing at a higher temperature (Holt and Fossheim 1981, Fossheim and Holt 1982).

5. Conclusions

From the discussion in the preceeding section, it should be clear that we are not able to arrive at a final conclusion in the understanding of our results. The explanation in terms of tricritical behaviour is the most appealing one, while the defect explanation may be the most probable one.

The present experiments are performed under zero external pressure. Thus the results may depend upon internal strains. Therefore future experiments of the same kind should be performed under application of external uniaxial or biaxial stresses, making it possible to investigate dynamic and static exponents at various points in the stress–temperature phase diagrams. Such experiments would hopefully confirm (or reject) the existence of tricritically influenced behaviour in unstressed $SrTiO_3$. We emphasise particularly in this context the importance of measuring both the velocity and attenuation at various frequencies and modes in the *same* sample.

Very little is known about the role of defects close to the phase transitions in these systems. Future experiments in samples where one controls the defect concentrations will therefore be of great importance in resolving some of the questions raised in § 4.

Acknowledgments

The authors wish to acknowledge Professor H J Scheel for supplying the flux-grown sample. K A Müller, R A Cowley and E H Hauge are acknowledged for useful comments.

References

Aharony A 1974 *Phys. Lett.* A **49** 221
Aharony A and Blankschtein D 1984 *Proc. (NATO ASI) on Multicritical Phenomena* eds R Pynn and A Skjeltorp (New York: Plenum) p 155
Aharony A and Bruce A D 1974 *Phys. Rev. Lett.* **33** 427
—— 1979 *Phys. Rev. Lett.* **42** 462
Bäuerle D and Rehwald W 1978 *Solid State Commun.* **27** 1343
Bell R O and Rupprecht G 1963 *Phys. Rev.* **129** 90
Berre B 1983 Private communication
Berre B and Fossheim K 1971 in *Structural Phase Transitions and Soft Modes* ed. E J Samuelsen, E Andersen and J Feder (Oslo: Universitetsforlaget)
Berre B, Fossheim K and Müller K A 1969 *Phys. Rev. Lett.* **23** 589
Bjerkan L, Fossum J O and Fossheim K 1979 *J. Appl. Phys.* **50** 5307
Blankschtein D and Aharony A 1981 *Phys. Rev. Lett.* **47** 439
Blankschtein D and Mukamel D 1982 *Phys. Rev.* B **25** 6939
Blume M 1974 *Anharmonic Lattices, Structural Transitions and Melting* ed. T Riste (Leiden: Noordhoff) p 245

Bruce A D and Aharony A 1975 *Phys. Rev.* B **11** 478
Bruce A D and Cowley R A 1981 *Structural Phase Transitions* (London: Taylor and Francis)
Buzaré J Y, Berlinger W and Müller K A 1984 *Preprint*
Clarke R 1978 *Phys. Rev.* B **18** 4920
Courdille J M and Dumas J 1969 *Solid State Commun.* **7** 1623
Courtens E 1976 *Local Properties at Phase Transitions*, ed. K A Müller and A Rigamonti (Amsterdam: North-Holland) p 293
D'iorio M, Berlinger W and Müller K A 1983 *Phase Transitions* **4** 31
Dohm V 1984 *Proc. (NATO ASI) on Multicritical Phenomena* eds R Pynn and A Skjeltorp (New York: Plenum) p 81
Domb E R, Schurmann H K and Mihalisin T 1976 *Phys. Rev. Lett.* **36** 1191
Fisher M 1974 *Rev. Mod. Phys.* **46** 597
Fossheim K 1984 *Proc. (NATO ASI) on Multicritical Phenomena* eds R Pynn and A Skjeltorp (New York: Plenum) p 129
Fossheim K and Berre B 1972 *Phys. Rev.* B **5** 3292
Fossheim K and Fossum J O 1984 *Proc. (NATO ASI) on Multicritical Phenomena* eds R Pynn and A Skjeltorp (New York: Plenum) p 113
Fossheim K and Holt R M 1978 *J. Phys. E: Sci. Instrum.* **11** 892
—— 1980 *Phys. Rev. Lett.* **45** 730
—— 1982 *Physical Acoustics* vol 16, ed. W P Mason and R N Thurston (New York: Academic)
Fossum J O 1985 *J. Phys. C: Solid State Phys.* **18** 5531
Fossum J O and Fossheim K 1984 *Ferroelectrics* **54** 289
Fossum J O, Fossheim K and Scheel H J 1984 *Solid State Commun.* **51** 839
Golding B 1970 *Phys. Rev. Lett.* **25** 1439
Halperin B I and Varma C M 1976 *Phys. Rev.* B **14** 4030
Hatta I, Shiroishi Y, Müller K A and Berlinger W 1977 *Phys. Rev.* B **16** 1138
Hikita T, Tsukahara T and Ikeda T 1982 *J. Phys. Soc. Japan* **51** 2900
Höchli U T and Bruce A D 1980 *J. Phys. C: Solid State Phys.* **13** 1963
Holt R M and Fossheim K 1981 *Phys. Rev.* B **24** 2680
Landau L D and Khalatnikov I M 1951 *Sov. Phys.–Dokl.* **96** 469
Leung R C, Zahradnick C and Garland C W 1979 *Phys. Rev.* B **19** 2612
Levanyuk A P, Osipov V V, Sigov A S and Sobyanin A A 1979 *Sov. Phys.–JETP* **49** 176
Lyons K B and Fleury P A 1977 *Solid State Commun.* **23** 477
Lüthi B and Moran T J 1970 *Phys. Rev.* B **2** 1211
Ma S 1976 *Frontiers in Current Physics* vol 46 (Reading, Mass.: Benjamin)
Mermin N D and Wagner H 1966 *Phys. Rev. Lett.* **17** 1133
Müller K A 1971 *Structural Phase Transitions and Soft Modes* ed. E J Samuelsen, E Andersen and J Feder, (Oslo: Universitetsforlaget) p 61
—— 1981 in *Nonlinear Phenomena at Phase Transitions and Instabilies*, ed. T Riste (New York: Plenum)
—— 1982 *Preprint* and private communication
Müller K A and Berlinger W 1982 *Z. Phys.* B **36** 81
Müller K A, Berlinger W, Drumheller J E and Bednorz J G 1984 *Proc. (NATO ASI) on Multicritical Phenomena* eds R Pynn and A Skjeltorp (New York: Plenum) p 143
Murata K K 1976 *Phys. Rev.* B **13** 4015
Nattermann T 1976 *J. Phys. C: Solid State Phys.* **9** 3337
Nattermann T and Trimper S 1975 *J. Phys. A: Math. Gen.* **8** 2000
Nava R, Callarotti R, Ceva H and Martinet A 1969 *Phys. Rev.* **188** 1456
Okazaki A, Ohama N, Willis B T M, Iwata Y, Scheel H J and Müller K A 1983 *Phase Transitions* **3** 339
Papadakis E P 1967 *J. Acoust. Soc. Am.* **42** 1045
Pfeuty P, Jasnow D and Fisher M E 1974 *Phys. Rev.* B **10** 208
Rehwald W 1970 *Solid State Commun.* **8** 607
—— 1977 *Solid State Commun.* **21** 667
Rehwald W and Lang G K 1975 *J. Phys. C: Solid State Phys.* **8** 3287
Reiter G F, Berlinger W, Müller K A and Heller P 1980 *Phys. Rev.* B **21** 1
Schwabl F 1974 *Anharmonic Lattices, Structural Transitions and Melting* ed. T Riste (Groningen: Noordhoff) p 87
Shapiro S M, Axe J D, Shirane G and Riste T 1972 *Phys. Rev.* B **6** 4332
Stokka S and Fossheim K 1981 *J. Phys. C: Solid State Phys.* **15** 1161
—— 1982 *Phys. Rev.* B **25** 4896
Töpler J, Alefeld B, Heidemann A 1977 *J. Phys. C: Solid State Phys.* **10** 635